Neoplasia 36 (2023) 100874

Contents lists available at ScienceDirect

Neoplasia

journal homepage: www.elsevier.com/locate/neo

Original Research

S-adenosylmethionine blocks tumorigenesis and with immune checkpoint inhibitor enhances anti-cancer efficacy against BRAF mutant and wildtype melanomas

A. Mehdi[a,b,g], M. Attias[a,c,h,i], A. Arakelian[g], M. Szyf[a,f], C.A. Piccirillo[a,c,h,i], S.A. Rabbani[a,b,d,e,g,*]

[a] Faculty of Medicine and Health Sciences, McGill University, Montreal, QC H3A 2B4, Canada
[b] Department of Human Genetics, McGill University, Montreal, QC H3A 2B4, Canada
[c] Department of Microbiology and Immunology, McGill University, Montreal, QC H3A 2B4, Canada
[d] Department of Experimental Medicine, McGill University, Montreal, QC H3A 2B4, Canada
[e] Department of Oncology, McGill University, Montreal, QC H3A 2B4, Canada
[f] Department of Pharmacology and Therapeutics, McGill University, Montreal, QC H3A 2B4, Canada
[g] Program in Metabolic Disorders and Complications (MeDiC), Research Institute of the McGill University Health Centre, 1001 Décarie Blvd. (Glen site), Room EM1.3232, Montréal, QC H4A 3J1, Canada
[h] Program in Infectious Diseases and Immunology in Global Health, Centre for Translational Biology, Research Institute of the McGill University Health Centre, Montréal, QC H4A 3J1, Canada
[i] Centre of Excellence in Translational Immunology (CETI), Montréal, QC H4A 3J1, Canada

ARTICLE INFO

Keywords:
S-adenosylmethionine
Immune checkpoint inhibitors
Anti-PD-1 antibody
Phenotype switching
MITF
Melanoma
YUMMER1.7
B16
Melanin

ABSTRACT

Despite marked success in treatment with immune checkpoint inhibitor (CPI), only a third of patients are responsive. Thus, melanoma still has one of the highest prevalence and mortality rates; which has led to a search for novel combination therapies that might complement CPI. Aberrant methylomes are one of the mechanisms of resistance to CPI therapy. S-adenosylmethionine (SAM), methyl donor of important epigenetic processes, has significant anti-cancer effects in several malignancies; however, SAM's effect has never been extensively investigated in melanoma. We demonstrate that SAM modulates phenotype switching of melanoma cells and directs the cells towards differentiation indicated by increased melanogenesis (melanin and melanosome synthesis), melanocyte-like morphology, elevated Mitf and Mitf activators' expression, increased antigen expression, reduced proliferation, and reduced stemness genes' expression. Consistently, providing SAM orally, reduced tumor growth and progression, and metastasis of syngeneic BRAF mutant and wild-type (WT) melanoma mouse models. Of note, SAM and anti-PD-1 antibody combination treatment had enhanced anti-cancer efficacy compared to monotherapies, showed significant reduction in tumor growth and progression, and increased survival. Furthermore, SAM and anti-PD-1 antibody combination triggered significantly higher immune cell infiltration, higher $CD8^+$ T cells infiltration and effector functions, and polyfunctionality of $CD8^+$ T cells in YUMMER1.7 tumors. Therefore, SAM combined with CPI provides a novel therapeutic strategy against BRAF mutant and WT melanomas and provides potential to be translated into clinic.

Introduction

There are 232,100 new cases of melanoma diagnosed and about 55,500 cancer deaths from melanoma annually [1]. Melanoma can be genetically stratified into four major subgroups; (1) activating BRAFV600 mutations (~50%); (2) N/H/K-RAS mutations (15–20%), (3) inactivating mutations of NF-1 (~10%), and (4) triple wild-type (WT)-WT BRAF, N/H/K-RAS and NF-1 (30–35 %) [2]. CPI therapy has shown long lasting responses in a group of patients and has led to a paradigm shift in treating all melanoma genotypes [3,4]. However, 60–70% of melanoma patients do not respond to CPI therapy due to mechanisms such as tumor-intrinsic lack of immunogenicity, immunosuppressive tumor microenvironment (TME) as well as innate and acquired resistance [5,6]. Therefore, there is an urgent need to develop novel combinational therapies that could complement CPI and improve melanoma related morbidity and mortality.

The resistance to CPI can stem from the heterogeneous nature of melanoma cells that switch between differentiated, highly proliferative,

* Corresponding author at: Program in Metabolic Disorders and Complications (MeDiC), Research Institute of the McGill University Health Centre, 1001 Décarie Blvd. (Glen site), Room EM1.3232, Montréal, QC H4A 3J1, Canada.
E-mail address: shafaat.rabbani@mcgill.ca (S.A. Rabbani).

https://doi.org/10.1016/j.neo.2022.100874
Received 1 November 2022; Received in revised form 27 December 2022; Accepted 28 December 2022

and invasive stem-cell like states [7–10]. While acting as a rheostat, microphthalmia-associated transcription factor (MITF), a master transcription factor, primarily controls phenotype switching of melanoma cells [7–10]. Increased MITF expression leads to low-proliferative terminally differentiated cells called melanocytes which produce melanin via melanogenesis [11]. Transcription factors, cAMP-response element binding protein (CREB) and SRY-box transcription factor 10 (SOX10), are activators that increase MITF expression and are also involved in melanogenesis [11,12]. MITF also increases transcription of tyrosinase (TYR) and tyrosinase related enzymes, TYRP-1, and TYRP-2, that convert tyrosine to melanin [11–13]. Moreover, premelanosome protein (PMEL or GP100) and Melanocyte antigen recognized by T cells (MART-1 or MELAN-A), genes required for melanogenesis and melanosome generation, are also regulated by MITF [11–14]. Reduction of MITF expression results in dedifferentiated melanomas that are resistant to therapies, highly invasive and metastatic, and causes reduced overall survival of patients [10,15,16]. Therefore, directing phenotype switching by modulating MITF levels has been suggested as an effective anti-melanoma therapy [7,9].

Melanocyte differentiation antigens (MDAs) are peptides generated from genes involved in melanogenesis and melanosome generation including TYR, TYRP-1, TYRP-2, MART-1 and PMEL [14]. Although MDAs are self-antigens, autologous cytotoxic T lymphocytes directed against MDAs, can mediate tumor regression, break tolerance to the tumor, and therefore are being evaluated as targets for anti-melanoma immunotherapy and in melanoma vaccines [14]. A major immune evasive mechanism is low intrinsic immunogenicity where tumor cells display reduced levels of immunogenic tumor antigens (or neoepitopes) [17]. Therefore, increasing expression of antigens such as MDAs and melanoma associated antigens (MAAs) can enhance immunogenicity of the tumor cells resulting in greater response in general and to CPIs [18,19].

The resistance to CPI has been associated with alterations in the methylome of cancer cells [20,21]. To distinguish CPI responders from non-responders, DNA hypomethylation was proposed as an essential biomarker for predicting tumor response to host immunity, and DNA hypomethylation could also provide a possible mechanism for immune escape and resistance to CPI [21]. Moreover, global hypomethylation levels were strongly associated with immune evasion signatures independently of aneuploidy and tumor mutational burden [21]. S-adenosylmethionine (SAM), a methyl donor of numerous epigenetic methyl transferases, was shown to counteract DNA hypomethylation and block DNA demethylation [22–24]. SAM has significant anti-cancer effects in various malignancies; however, SAM's effect has not been extensively investigated in melanoma. Interestingly, SAM is also crucial for activation, proliferation, and survival of T cells [25–29]. Furthermore, SAM levels are reduced by cancer cells via several mechanisms in TME [30,31]. Consistently, the depletion of methionine (the pre-cursor of SAM) in TME results in $CD8^+$ T cells becoming dysfunctional and $CD8^+$ T cells become unresponsive to CPI [30]. This is another essential immune evasive mechanism used by tumor cells [30].

We have previously tested the effect of SAM and anti-PD-1 antibody combination on tumor growth of a syngeneic BRAF WT mouse model and found enhanced anti-cancer efficacy of the combination treatment. However, the effect of SAM alone and in combination with anti-PD-1 antibody along with molecular pathways involved were not extensively investigated in melanoma, in general, and in the BRAF mutant melanoma which represents 50% of patients. Hence, we tested the hypothesis that SAM elevates anti-cancer immune responses, in addition to having anticancer effects, and that an effective novel therapeutic strategy for both BRAF mutant and WT melanoma would be to combine SAM and CPI. We show here using cancer cell lines and mouse models that SAM has significant anti-cancer effects on BRAF mutated and WT melanomas. The anti-cancer effect of SAM involves marked inhibition of cell proliferation and directing phenotype switching of invasive and proliferative melanoma cells into differentiated state. We also show that SAM and anti-PD-1 antibody combination has enhanced anti-cancer efficacy in reducing tumor growth and metastasis, and increasing survival in melanoma mouse models. The combination also markedly elevated adaptive immune responses indicated by a higher immune cell infiltration, higher $CD8^+$ T cells infiltration, activation, and effector functions, and higher polyfunctional $CD8^+$ T cells in TME of YUMMER1.7 tumors. Lastly, the combination also enhanced the frequency and functionality of $CD4^+$ T_h1 cells and reduced immunosuppressive $CD4^+$ $FoxP3^+$ T_{regs} in TME of YUMMER1.7 tumors.

Results

SAM has marked anti-proliferative effects on melanoma cells

Uncontrolled cellular proliferation is a major hallmark of cancer [32]. Firstly, to determine the anti-cancer effect of SAM, we tested the effect of SAM on proliferation in human (A375) and murine (YUMM1.7, B16 and YUMMER1.7) melanoma cell lines. B16 is a BRAF WT while YUMM1.7, YUMMER1.7 and A375 are BRAF mutant cell lines. While SAM decreased cell proliferation in all cell lines in a dose-dependent manner relative to control, the effect was greatest on YUMMER1.7 cell line at both SAM 200μM and 500μM doses, followed by YUMM1.7, B16, and A375, respectively (Fig. 1A).

Next, to determine the key players that regulate cell cycle progression in melanoma, we analyzed major cell cycle regulators that are differentially expressed in human melanoma primary tumor, metastatic and normal skin tissues using the Xena platform [33]. Key cell cycle regulators including inhibitors such as p21 had low expression in primary tumors and metastatic tissue compared to normal skin tissue (Fig. 1B). In contrast, cell cycle dependent kinases and cyclins that drive cell cycle forward such as CDK1, CDK2 and CCNB1/2 had higher expression in primary tumors and metastatic tissues compared to normal skin tissue (Fig. 1C). Importantly, treatment of YUMMER1.7 and B16 cells with SAM reversed the expression of most of the cell cycle regulators tested (Fig. 1D and Supplementary Fig. 1). For instance, p21 which was highly expressed in the human primary tumors and metastatic tissue was significantly upregulated by SAM in YUMMER1.7 cells and vice versa for CDK1, CDK2 and CCNB1/2 expression (Fig. 1D).

RNA-sequencing of YUMMER1.7 cells treated with SAM (200μM and 500μM) revealed many differentially expressed genes (DEGs) upon SAM treatment at 200μM (up, 3715; and down, 3557 genes) and 500μM (up, 4235; and down, 3935 genes) (Supplementary Fig. 2A). We carried out pathway analysis of DEGs using GSEA (Supplementary Fig. 2B and C, 3 and 4 and Supplementary Tables 3 and 4). Importantly, key cell cycle pathways and pathways involved in translation and related processes were significantly downregulated upon SAM (500μM) treatment in YUMMER1.7 cells indicating marked cell cycle inhibition (Supplementary Figs. 2B and 3, and Supplementary Table 5).

Next, we overlapped the DEGs obtained from SAM treatment with the known melanoma driving genes (n = 422) of the Melanoma Gene Database (MGDB) and found 47% of genes to be common between the MGDB and DEGs obtained after treatment with SAM (500μM) (Supplementary Fig. 2D) [34]. Expectedly, pathway analysis of common genes revealed Melanoma and core cancer pathways enrichment (Supplementary file 1). Together, these results indicate that SAM regulates core genes/pathways in melanoma tumorigenesis and inhibits cell cycle pathways thereby reducing cellular proliferation of melanoma cells.

SAM increases melanin and melanosome synthesis of melanoma cells

Upon treatment of B16 cells with SAM, we noticed that B16 cells appear darker suggesting increased melanin synthesis. Since melanin pigmentation was reported to affect melanoma behaviour, we investigated the effect of SAM on melanogenesis and melanosome formation [11,35,36]. B16 cells produce melanin and phenotypically recapitulates clinical features of human melanoma [37]. The ability to produce melanin is lost upon subsequent cycles during *in vitro* cell culturing. We

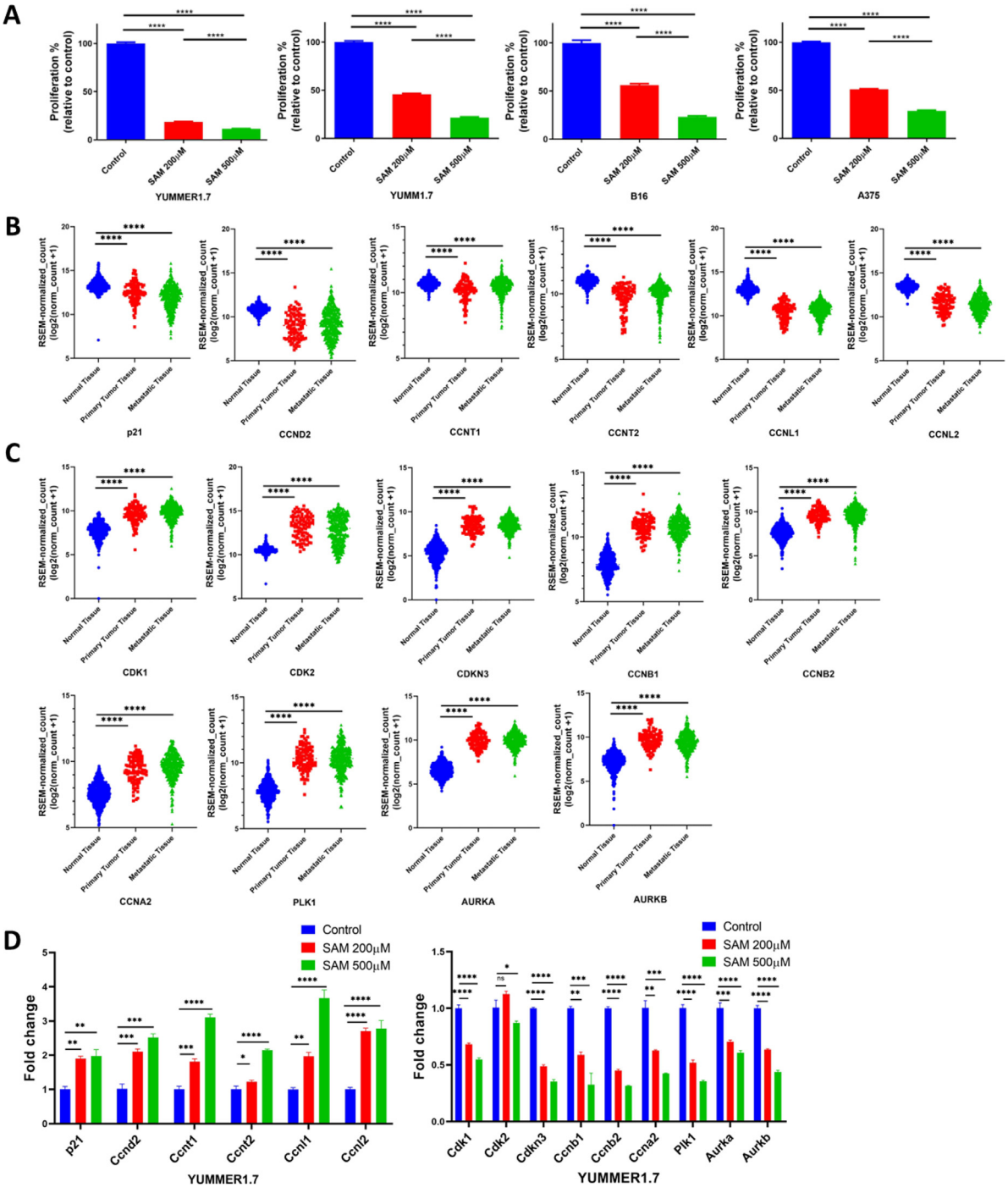

Fig. 1. SAM decreases cell proliferation of human and murine melanoma cell lines via modulating expression of key cell cycle regulators. (A) Effect of SAM on cell proliferation of melanoma cell lines. YUMMER1.7 (1×10^4 cells), YUMM1.7 (0.5×10^4 cells), B16 (1.5×10^4 cells) and A375 (2.5×10^4 cells) were seeded in 6-well plates and treated with two doses of SAM, 200μM and 500μM. Proliferation is represented as the percentage of proportion to Control (± SEM). (B-C) Expression of key cell cycle regulators in normal skin, primary tumor and metastatic tissue of human melanoma patients and normal healthy individuals extracted from TCGA and GTEx databases using Xena platform [33]. The expression data of genes has been plotted in a scatter-plot graph (1024 samples). (D) Expression of cell cycle regulators in YUMMER1.7 cells after treatment with two doses of SAM, 200μM and 500μM as determined using RT-qPCR. Expression is depicted as fold change (± SEM) relative to control. Statistical significance was calculated using (A-D) one-way ANOVA test.

took advantage of this and treated non-pigmented B16 cells with varying concentrations of SAM (200-500μM). Increase in SAM concentration induced melanogenesis as B16 cells had increased black pigmentation in a dose-dependent manner (Fig. 2A and B). Furthermore, the number of melanosomes and melanin synthesizing B16 cells were elevated as well (Fig. 2A). To measure the amount of intracellular melanin, we extracted the melanin from cells and measured absorbance. Treatment with SAM showed a gradual increase in endogenous (intracellular) melanin production in a dose dependent manner (Fig. 2B). We also observed slight increase in exogeneous (extracellular) melanin that changed the medium color from red to reddish black in wells treated with SAM (data not shown).

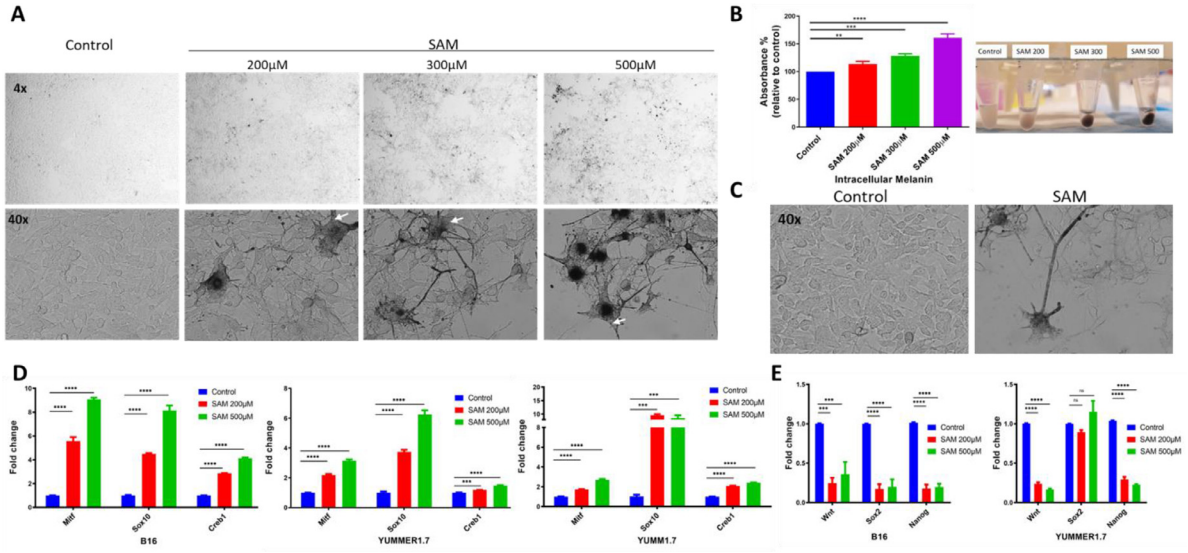

Fig. 2. SAM increases melanogenesis and drives phenotype switching of melanoma cells. (A) Microscope images (top; lens, 4x, magnification, 40x; and bottom; lens, 40x, magnification, 400x) showing effect of SAM on melanin and melanosome synthesis of B16 cells. B16 (1.5×10^4) cells were seeded in 6-well plates and treated with vehicle or SAM (200μM, 300μM and 500μM). Melanosomes can be viewed as dots (indicated by white arrows). (B, left) Percentage absorbance (relative to Control) of intracellular melanin extracted from B16 cell pellets treated with varying doses of SAM (200-500μM). Absorbance (± SEM) was measured at 490nm which is optimal wavelength for measuring melanin pigment. (B, right) Cell pellets showing SAM increases melanin of B16 cells in a dose dependent manner. (C) Images (lens, 40x, magnification, 400x) of B16 cells treated with control and SAM (200μM) showing morphological changes upon SAM treatment. (D-E) Expression of (D) melanocyte transcription factors (TFs) and; (E) master CSC marker genes (*Wnt, Sox2* and *Nanog*); in melanoma cell lines upon treatment with SAM (200 and 500 μM) analyzed with RT-qPCR. Expression is depicted as fold change (± SEM) relative to control. Statistical significance was calculated using (B, D, E) one-way ANOVA test.

SAM regulates phenotype switching of melanoma cells through modulating Mitf expression

Melanocytes are thin, elongated cells with branched structures, consisting of a central body and dendrites, and contain numerous melanin-containing melanosomes [12,38,39]. Whereas B16 cells are a mixture of short spindle-shaped and epithelial-like cells lacking dendrites, and loose pigmentation (Control group, Fig. 2C). Treatment with SAM resulted in differentiation of B16 cells into melanocyte-like cells (Fig. 2C). These differentiated cells were thin, dark black stained, and had more melanosomes and dendrites (Fig. 2C). Furthermore, in heterogeneous B16 cell population, a higher number of B16 cells appeared melanocyte-like cells in increasing SAM dose from 200μM to 500μM (Fig. 2A). Moreover, the differentiated cells also had reduced proliferative ability (Figs. 1A and 2A).

MITF loss or low expression can lead to dedifferentiated melanomas that are resistant to therapies, are highly invasive and metastatic, and results in reduced overall survival of patients [10,15,16]. In addition to its clinical significance, MITF is also the master regulator of melanogenesis and hence we investigated its expression. SAM elevated *Mitf* expression by several folds in all the melanoma cell lines that we tested in a dose-dependent manner (Fig. 2D). *Mitf* was also found to be significantly upregulated upon SAM treatment in RNA-seq data and was a common gene between DEGs upon SAM treatment and the MGDB database. Interestingly, 126 MITF target genes were also differentially expressed in response to SAM treatment (Supplementary Fig. 2E) [40]. Moreover, the transcriptional activators *Sox10* and *Creb1*, which induce *Mitf* expression, melanogenesis, and differentiation phenotype, were also increased several folds by SAM (Fig. 2D).

Cancer stem cells (CSCs) or melanoma initiating cells (MICs) have high expression of stemness marker genes including *NANOG, WNT, SOX2*, and in some studies, *BRN2* (*Pou3f2*) and *SLUG* (*Snai2*) [9,41,42]. We found that SAM caused significant reduction in essential MICs marker genes including *Nanog* and *Wnt* expression in both B16 and YUMMER1.7 cells, and significant downregulation of *Sox2* expression in B16 cells (Fig. 2E). *Brn2* was also significantly downregulated in B16 and YUMMER1.7 cells, and *Slug* in B16 cells (Supplementary Fig. 5). This indicates that SAM reduces the proportion of MICs in heterogeneous melanoma cell population and redirects MICs from dedifferentiated state towards a differentiated phenotype.

SAM increases immunogenicity and sensitivity of melanoma cells to CPIs

Since melanogenesis involves expression of melanocyte differentiation antigens (MDAs) and recognition of antigens including MDAs is central to immune response and immunotherapy against melanoma, we next determined the effect of SAM on expression of MDAs. Expectedly, SAM increased expression of most MDAs (*Tyr, Tyrp1, Tyrp2/Dct, Mart-1/Melan-A, Pmel/Gp100*) directly involved in melanogenesis by several folds in B16 and YUMMER1.7 cells (Fig. 3A). As expected, YUMMER1.7 and YUMM1.7 cell lines that do not produce melanin had no/undetectable expression of *Tyr* (Fig. 3A). Expression of *Tyrp1* and *Mart-1* was also upregulated by SAM while *Tryp2* expression was undetectable in YUMM1.7 cells (Fig. 3A).

In addition to MDAs expression, SAM (200μM and 500μM) also increased the expression of melanoma associated antigens (MAAs) including chondroitin sulfate proteoglycan 5 (*Cspg5*), melanoma inhibitory activity (*Mia*), somatostatin receptor 2 (*Sstr2*), melanoma cell adhesion molecule (*Mcam*), proteoglycan 4 (*Prg4*) and melanoregulin (*Mreg*) in YUMMER1.7 cells (Fig. 3B) except *Cspg5* at SAM 200μM [14]. In addition, tumor associated antigens (TAAs), such as the cadherins, adhesions and S100 family genes were also upregulated by SAM in YUMMER1.7 cells (Supplementary Fig. 6). Consistently, pathways that generate high neoepitopes such as oxidative stress, ROS, NRF2, UV response and other related pathways were found to be the top significantly upregulated pathways upon SAM treatment (Supplementary Fig. 2C and 4, and Supplementary Table 6).

Since immune checkpoints play a key role in anti-cancer or pro-cancer immune responses, we tested the expression of several immune checkpoint molecules including PD-L1 (*Cd274*), PD-L2 (*Cd273*), *Cd47*,

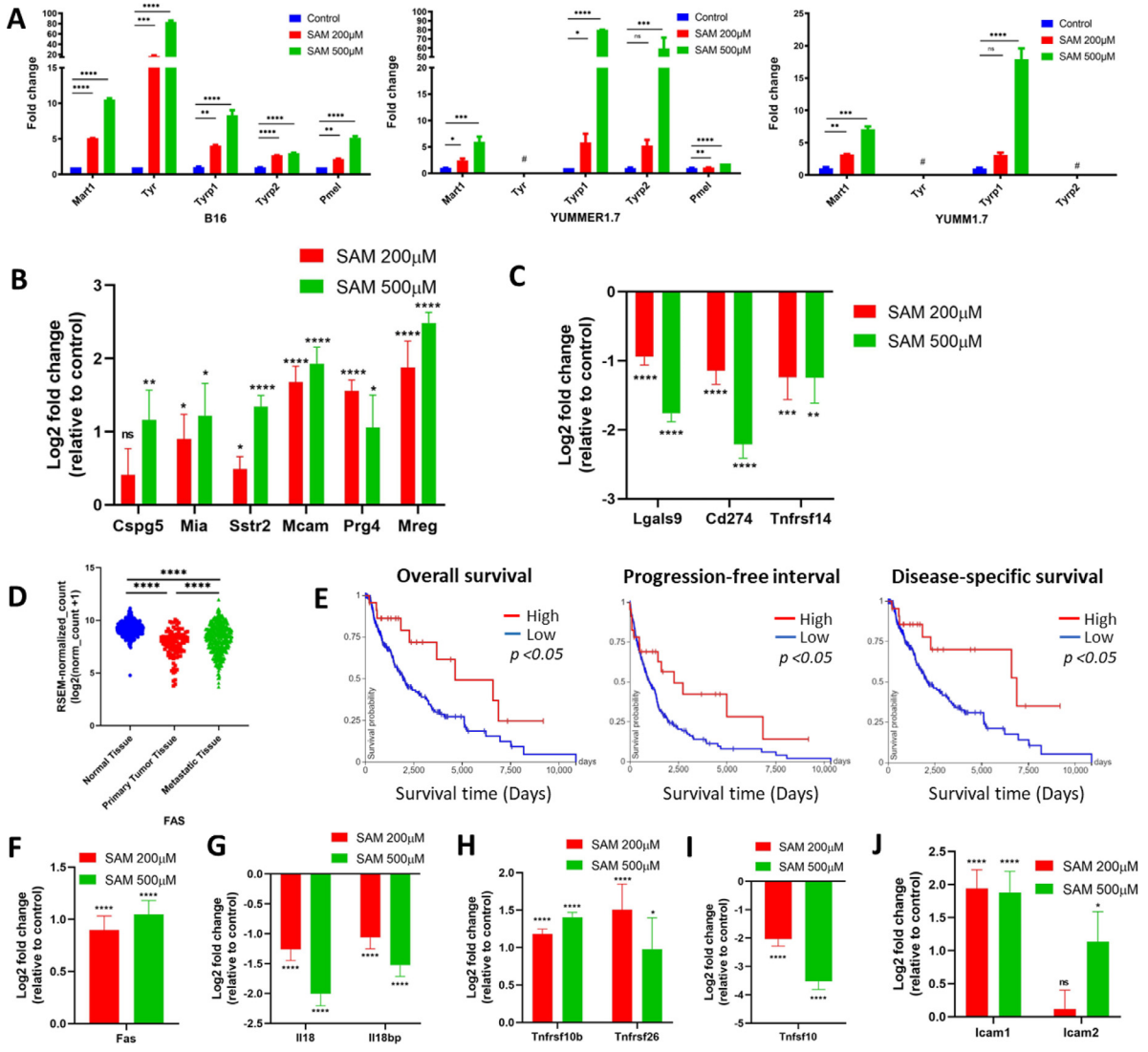

Fig. 3. SAM increases immunogenicity of murine melanoma cell lines. (A) Expression of melanocyte differentiation antigens (MDAs) in B16, YUMMER1.7 and YUMM1.7 cells upon treatment with SAM (200 and 500μM) analyzed with RT-qPCR. # *Tyr* had no/undetectable expression in non-pigmented YUMMER1.7 and YUMM1.7 cells while *Tryp2* expression was also undetectable in YUMM1.7 cells. Expression is depicted as fold change (± SEM) relative to control. Statistical significance was calculated using one-way ANOVA for each gene. (B-C) Expression of (B) melanoma associated antigens (MAAs); and (C) immune inhibitory molecules in YUMMER1.7 cells upon treatment with SAM (200 and 500μM) extracted from RNA-seq data. The log2 fold change is relative to Control where value of control is 0. The FDR values are placed on top of each bar and are relative to control. (D) Expression of *FAS* in the normal skin tissue, primary tumor and metastatic tissue samples of healthy and melanoma patients (n=1024 samples) extracted from GTEx and TCGA databases, respectively, and produced using Xena [33]. RSEM (RNA-Seq by Expectation Maximization) represents expression values. (E) Overall survival, progression-free interval and disease specific survival Kaplan Meier curves of *FAS*; X-axis: survival time (days); Y-axis: probability of survival. (E, left) Low (blue) n= 248; High (red) n = 23; $P = ^{*}$. (E, middle) Low (blue) n= 249; High (red) n = 23; $P = ^{*}$. (E, right) Low (blue) n= 244; High (red) n = 22; $P = ^{*}$. Survival plots were produced using Xena. (F-J) Expression of (F) *Fas* receptor;(G) *Il18* and *Il18bp*; (H) TRAIL receptors (*Tnfrsf10b, Tnfrsf26*); (I) TRAIL ligand (*Tnfsf10*); and (J) *Icam1* and *Icam2* genes in YUMMER1.7 cells upon treatment with SAM (200 and 500 μM) extracted from RNA-seq data. The log2 fold change is relative to Control where value of control is 0. The FDR values are placed on top of each bar and are relative to control. Statistical significance was calculated using (A, D) one-way ANOVA test; (B, C, F-J) Wald test with BH FDR.

cytotoxic T-lymphocyte-associated protein 4 (*Ctla4)*, galectin-9 (*Lgals9*), Nectin2/3 (*Cd112/113*), T Cell Immunoreceptor with Ig and ITIM Domains (*Tigit*), herpes virus entry mediator (*HVEM* or *Tnfrsf14*), and T cell immunoglobulin and mucin-domain containing-3 (*Tim-3* or *Havcr2*). We found that immune inhibitory molecules including PD-L1, galectin-9 and HVEM were significantly downregulated in SAM-treated (200μM and 500μM) YUMMER1.7 cells compared to control (Fig. 3C).

Both FAS death receptor (FAS/Apo1) and its ligand (FASL/Apo1L), and TRAIL death receptors (TNFRSF10-A/B/C/D or TRAIL-R1/2/3/4) and its ligand (TNFSF10/Apo2L), are major apoptosis pathway that causes instant cell death [43–45]. The lack of expression of FAS and TRAIL receptors in tumors can result in immune evasion and is correlated with poor prognosis of malignant melanomas, whereas increased FAS and TRAIL receptor expression in tumors can result in killing by cytotoxic $CD8^{+}$ T and NK cells [45–48]. Importantly, we found significantly lower expression of *FAS* receptor in primary tumors and metastatic tissues of melanoma patients as compared to normal skin tissue samples, and this was associated with lower overall survival, progression-free interval, and disease-specific survival (Fig. 3D–E). Interestingly, we found SAM significantly increased expression of *Fas* receptor in YUMMER1.7 cells (Fig. 3F). Additionally, SAM lowered expression of genes *Il18* and *Il18bp* in YUMMER1.7 cells which were previously shown to have a crucial role in survival of B16 melanoma cells and inhibit Fas/FasL pathway and NK mediated killing (Fig. 3G) [49].

Furthermore, SAM resulted in significant upregulation of major TRAIL receptors including TRAIL-R2 (*Tnfrsf10b*), TRAIL-R1/3 (*Tnfrsf26* or *Tnfrsf1/3*) whereas downregulation of TRAIL ligand (*Tnfsf10*) expression in YUMMER1.7 cells (Fig. 3H-I). In addition, SAM also increased TWEAKR receptor (*Tnfrsf12a*) and *Tnfrsf18* expression (Supplementary Fig. 7). Consistently, FAS, apoptosis, TNF pathways and immune stimulating pathways (including T cell TCR signalling) were upregulated in YUMMER1.7 cells treated with SAM (Supplementary Table 7).

Intercellular adhesion molecule 1 (ICAM-1) is an essential antigen present on antigen presenting cells (APCs) or tumor cells that interacts with lymphocyte function associated antigen 1 (LFA-1) which is a major co-stimulatory molecule present on T cells. LFA-1/ICAM-1 interactions are essential for trans-endothelial migration of $CD8^+$ T cells into TME, and $CD8^+$ T cells initial activation and lytic functions [50–52]. Moreover, ICAM-1 overexpression on tumor cells have been reported to cause reduction in tumor growth [53,54]. Parallel to the increase in Fas, TRAIL receptors and immunostimulatory antigens' expression, *Icam1* (200μM and 500μM) and *Icam2* (500μM only) were also significantly upregulated by several folds upon SAM treatment (Fig. 3J).

Collectively, these data show that SAM alters melanoma transcriptome that is consistent with increased immunogenicity and sensitivity of melanoma cells to CPIs.

SAM modulates Mitf expression that further regulates phenotype switching

Next, to elucidate a potential mechanism for upregulation of antigens upon SAM treatment, we examined a direct involvement of the *Mitf* transcription factor. Therefore, we knocked down (KD) *Mitf* using siRNA targeting the *Mitf* gene (siMitf) at 3 sites simultaneously and confirmed that *Mitf* expression was markedly downregulated (Fig. 4A). Most of the MDAs' expression was downregulated upon siMitf KD indicating that Mitf is an important transcription factor controlling the expression of these MDAs (Fig. 4A). Parallel to the effect of SAM elevating *Mitf* levels, KD of *Mitf* expression significantly increased expression of stemness genes including *Nanog, Wnt* and *Sox2* in B16 and YUMMER1.7 cells (Fig. 4B). Hence, showing that *Mitf* induction is critical for its effect on melanogenesis and differentiation.

Collectively, these data suggest that SAM modulates the phenotype switching of melanoma cells. Treating melanoma cells with SAM switches proliferative and invasive stem-cell phenotype towards more differentiated state indicated by low proliferative ability, melanocyte-like cell morphology, elevated melanogenesis, decreased stemness ability and increased immunogenicity (Fig. 4C).

SAM reduces tumor growth, progression, and metastasis of melanoma tumors

To determine effect of SAM *in vivo,* we established either YUMMER1.7 or B16 tumors in immunocompetent B6 mice and treated them with either control (PBS) or SAM (80mg/kg/day) via oral gavage. SAM treatment significantly reduced tumor growth and progression in both mouse models compared to control (Fig. 5A).

Expression of nuclear protein Ki67 (Ki67) is strongly associated with various tumor parameters including growth, progression, clinical tumor stage, metastasis, and is the most extensively used proliferation marker [55]. Consistent with SAM reducing proliferation and causing cell cycle inhibition, SAM had a significant decrease in Ki67-positive stained tumor cells indicating marked reduction in proliferation, growth, and progression of YUMMER1.7 and B16 tumors (Fig. 5B). Moreover, parallel to *in vitro* results, SAM also showed a significant elevation in *Mitf* and MDAs (such as *Mart-1* and *Pmel*) expression in both YUMMER1.7 and B16 tumors (Fig. 5C).

Both melanosomes and melanin pigmentation have shown to significantly inhibit melanoma metastasis (*in vivo*) [35,36]. SAM increased melanin and melanosome production, increased *Mitf* expression and reduced the pool of invasive MICs in B16 heterogenous population. Considering this, we investigated the effect of SAM in a model of B16 melanoma lung metastasis through intravenous administration of B16 cells. The mice treated with SAM had significant decrease in proportion of lung metastatic nodules compared to control lungs (Fig. 5D). Moreover, treatment of SAM decreased cell migration of YUMMER1.7 and A375 cells in a wound-healing assay (*in vitro*) (Supplementary Fig. 8). Additionally, SAM reduced invasiveness of B16 cells as shown by us previously [22]. Taken together, these results suggest that SAM can significantly reduce the metastatic potential of melanoma.

SAM and anti-PD-1 antibody combination has superior anti-cancer efficacy against melanoma tumors

Based on our data above, we further hypothesized that treatment with SAM would complement with CPI therapy. We treated YUMMER1.7 tumor bearing mice with control (IgG and oral PBS), SAM, anti-PD-1 antibody, and combination of both. Both SAM and anti-PD-1 antibody alone had significant effect in reducing tumor growth and progression as indicated by lower mean tumor volume and high tumor growth inhibition (TGI) (74.4% and 72.0% at day 22), compared to control (0%), respectively (Fig. 6A and B). However, SAM+anti-PD-1 combination had significantly high efficacy in blocking tumor growth and progression compared to all other groups indicated by lowest mean tumor volume and maximum TGI (88.6%) at day 22 (Fig. 6A and B).

Moreover, mice treated with SAM+anti-PD-1 combination had significantly highest survival probability (100% (10/10) at day 34 and median survival of 62 days), followed by anti-PD-1 antibody (60% (6/10) at day 34 and median survival of 46 days), SAM (50% (4/8) at day 34 and median survival of 35.5 days) and control (0% (0/8) at day 30 and median survival of 23 days) (Fig. 6C). Intriguingly, 20.0% (2/10) of the combination group mice had complete tumor elimination by the end of the study compared to anti-PD-1 antibody (10.0%, (1/10)), SAM (0.0%, 0/8), and control (0.0%, 0/8) (Fig. 6D).

We also tested SAM+anti-PD-1 antibody combination effect on lung metastasis (Fig. 6E). We found that SAM+anti-PD-1 had a larger effect on reducing lung metastasis as compared to all other groups (Fig. 6E). Taken together, these data suggest that SAM and anti-PD-1 antibody combination can significantly reduce tumor growth, progression, and metastasis of melanoma.

SAM and anti-PD-1 antibody combination elevates the infiltration, effector functions and polyfunctionality of $CD8^+$ T cells in the TME

To further understand the significant reduction in tumor growth and progression by SAM, anti-PD-1 antibody, and the combination, immunophenotyping of the tumors from YUMMER1.7-tumor bearing mice was carried out. Despite considerable inter-individual variability within each group, there were significantly higher levels of immune infiltration in the tumors treated with either SAM, anti-PD-1 antibody, or SAM+anti-PD-1 combination compared to control tumors (Supplementary Fig. 9). Similarly, the density of $CD3^+$ T cells was increased in all treatment groups (Fig. 7A). Furthermore, their proportion amongst tumor-infiltrating immune cells was increased and correlated inversely with tumor weight (Fig. 7A and Supplementary Fig. 10).

Cytotoxic $CD8^+$ T cells are the most powerful effectors in the adaptive anti-cancer immune response and increased $CD8^+$ T cell activation and function are hallmarks of response to PD-1 blockade [56]. Hence, we investigated the effect of the treatments on $CD8^+$ T cells' tumor infiltration, activation, and effector functions. Significantly higher densities and frequency of $CD8^+$ T cells infiltrated tumors of mice treated with SAM+anti-PD-1 antibody combination compared to control (Fig. 7B). The infiltrated $CD8^+$ T cells had higher activation levels in the SAM+anti-PD-1 antibody combination group as indicated by increased expression of the stimulatory checkpoint molecule ICOS both in terms of frequency and level of expression. Furthermore, this phenotype was

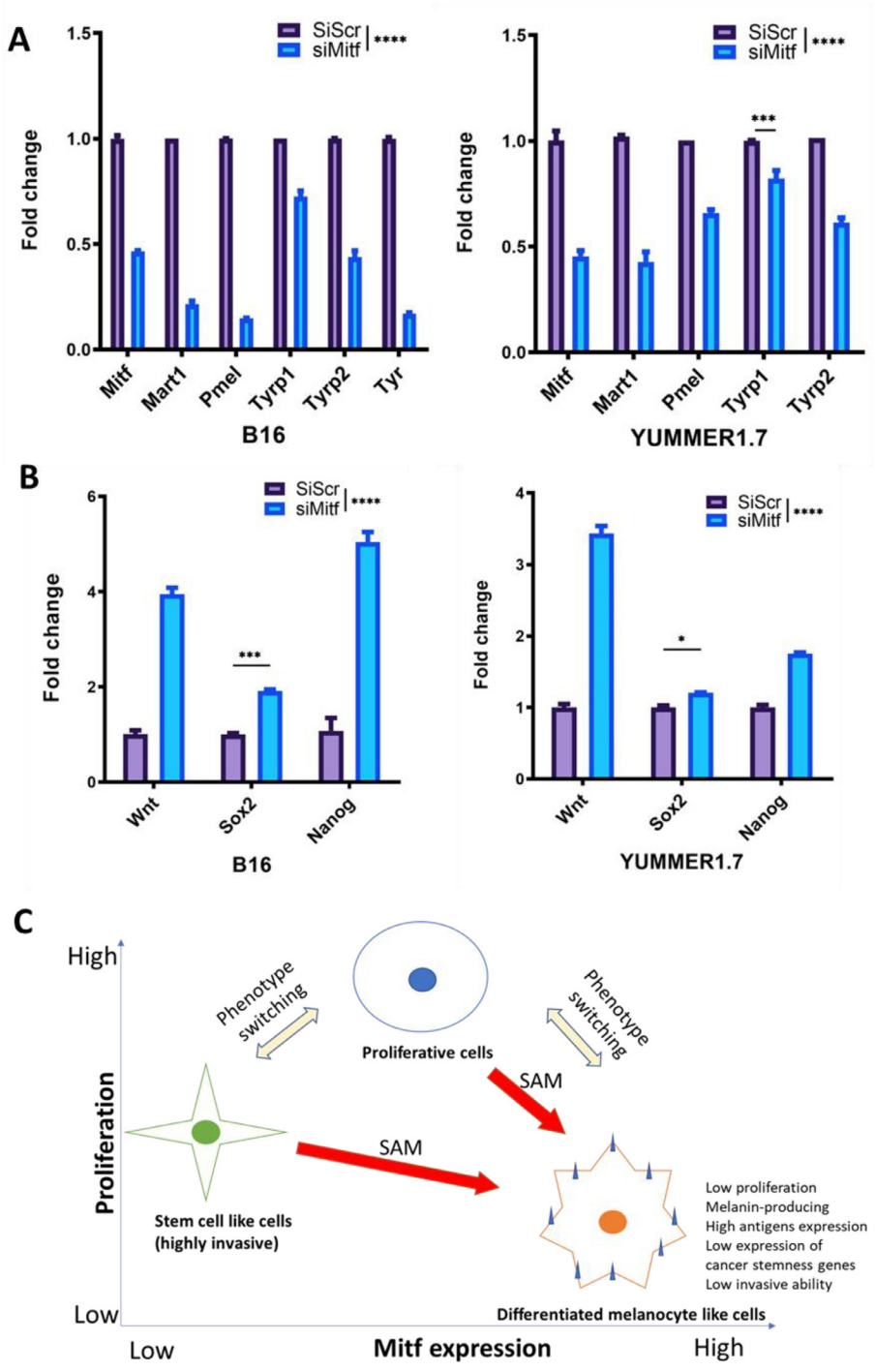

Fig. 4. *Mitf* is responsible for phenotype switching and controls the expression of MDAs and stemness genes in melanoma cells. (A-B) Expression (±SEM) of (A) *Mitf* and MDAs; and (B) master CSC marker genes (*Wnt, Sox2* and *Nanog*); in B16 and YUMMER1.7 cells upon siMitf (35nM) treatment analysed using RT-qPCR. The fold change is relative to scramble control (siScr) where value of control is 1. Statistical significance was calculated using (A-B) two-way ANOVA test and are **** unless indicated. (C) Model figure summarizing the effect of SAM on phenotype switching of melanoma cells from invasive and proliferative to differentiated state which could be due to elevation in Mitf levels.

inversely correlated with tumor weight (r^2 = 0.34) (Fig. 7C). Expression of the transcription factor T-bet, which is an indicator of $CD8^+$ T cells activation and effector functions, was increased in the combination group compared to control as well (Fig. 7D).

CPIs were designed to counteract the exhaustion of tumor-infiltrating T cells, a state caused by chronic activation and characterized by high levels of PD-1 signaling and loss of effector functions such as cytokine-secreting capacity [56]. This feature was recapitulated in the control tumors, with high proportions of PD-1 expressing cells (Supplementary Fig. 11) and absence of polyfunctional cells secreting both IFNγ and TNFα (Fig. 7E), a subset of $CD8^+$ cells considered as the most cytotoxic and the most potent effector of anti-tumor immunity [57]. Accordingly, the $CD8^+$ T cells in the TME of combination group produced significantly higher levels of T-bet (Fig. 7D), which promotes CD8 effector function such as the expression of IFNγ, and cytokines including IFNγ and TNFα compared to control group (Fig. 7E). Moreover, polyfunctional $CD8^+$ cells were observed in higher frequency and density in the combination group and represented up to 60% of $CD8^+$ cells in the mice with lowest tumor burden (Fig. 7E).

In general, SAM group had a higher density of infiltrating $CD8^+$ T cells (Fig. 7A, B, $p<0.05$), activation (MFI of $ICOS^+$ and T-bet^+ density; $p<0.05$; Fig. 7C and D), and a non-significant trend towards higher cytokine expression (IFNγ and TNFα; Fig. 7E; $p>0.05$) and polyfunctionality (Fig. E; $p>0.05$) compared to control. This is in line with SAM increasing the immunogenicity (antigen expression) of melanoma cells and tumors (Figs. 3 and 5) which would ultimately lead to higher acti-

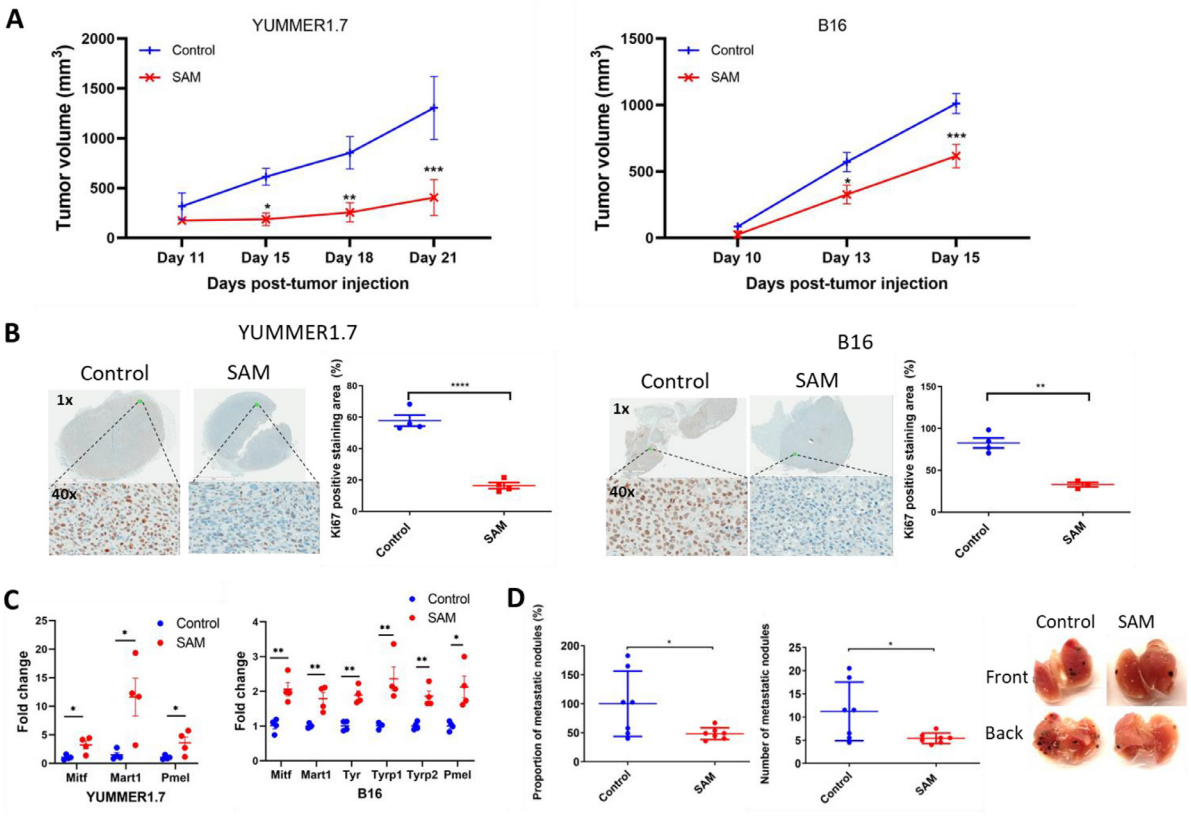

Fig. 5. SAM reduces tumor growth and progression, and metastasis of melanoma mouse models. (A) Tumor volume (mm^3) of control (PBS) and SAM treated YUMMER1.7 (n≥7/group) and B16 (n≥10/group) tumor bearing mice plotted against days post tumor injection. Data pooled from two independent repeats. Essentially, YUMMER1.7 (5×10^5) and B16 (5×10^5) cells were subcutaneously injected in C57BL/6 mice, and once the tumors were palpable treatment was initiated with either control (PBS) or SAM via oral gavage. Tumor volumes were measured at timed intervals. (B, left) Immunohistochemical images (top; lens, 1x, magnification, 10x; and bottom; lens, 40x, magnification, 400x) of the primary YUMMER1.7 (n=4 samples/group) and B16 (n≥3 samples/group) tumors stained with murine antibody against Ki67 proliferation marker (brown) from control and SAM treated group showing proliferative ability of tumor cells. The nucleus is stained blue. (B, right) Ki67 positive staining area percentage (n= 5 images/sample ±SEM). (C) Expression (±SEM) of *Mitf* and MDAs in YUMMER1.7 and B16 tumors from control and SAM treated group (n=4 samples/group) determined with RT-qPCR. (D) Percentage proportion of metastatic nodules (relative to control, ±SEM) and number of metastatic nodules (±SEM) on lungs of control and SAM treated mice. Representative lung images showing front and back. Essentially, B16 (2.5×10^5) cells were intravenously injected in C57BL/6 mice (n≥ 7/group) and treated with PBS (control) or SAM. Statistical significance was calculated using (A) two-way ANOVA test; (B-D) two-tailed t-test.

vation and effector functions of antigen-specific $CD8^+$ T cells. Indeed, loss of MDAs (MART-1, TYR) due to mutation or KD results in increased tumor volume in immunocompetent mice [16,58].

SAM-mediated protection correlates with augmented $CD4^+$ T helper responses in melanoma tumors

Consistently, all treatment groups had a significantly higher density and frequency of infiltrating $CD4^+$ T cells compared to the control group (Fig. 8A, $p<0.05$), in the TME. In the combination group, there was a significant shift in the composition of the $CD4^+$ T cell pool with reduced accumulation of $Foxp3^+$ T_{reg} cells and an increase in the frequency of T-bet^+ T_h1 cells (Fig. 8B and C). Furthermore, the functionality of these T_h1 cells was increased in the combination group, as shown by the increased frequency of IFNγ and TNFα which correlated inversely with tumor volume (Fig. 8C).

Surprisingly, we observed the presence of a subset of $CD4^+$ $IL17^+$ T cells in groups treated with SAM (SAM and SAM+anti-PD-1) which was absent in the control and anti-PD-1 antibody group (Fig. 8D). These cells were confirmed as bona fide Th17 cells through RORγt co-expression and absence of T-bet and IFNγ expression (Fig. 8C, D). Furthermore, expression of *IL-6,* a cytokine known to promote Th17 polarization in the presence of TGFβ [59], was markedly increased in YUMMER1.7 cells cultured with SAM *in vitro* (Supplementary Fig. 12). IL-17 responses have not been associated with response to checkpoint blockade in melanoma, and the frequency of Th17 did not correlate with tumor volume in the groups that received SAM (Fig. 8D). However, in other tumor types, Th17 cells contribute to the recruitment of $CD4^+$ and $CD8^+$ T cells into TME, and activation of tumor-specific $CD8^+$ T cells [60]. In accordance with this data, the expression of *Icam1* which is essential for trans-endothelial migration and lytic functions of $CD8^+$ T cells, was upregulated by several folds by SAM in YUMMER1.7 cells (Fig. 3H) [70–72].

Taken together, these data indicate that combining SAM with anti-PD-1 antibody treatment provides no additional benefit in terms of recruitment of $CD8^+$ and $CD4^+$ T cells in the TME, however, the difference was in higher activation and effector functions of both $CD4^+$ and $CD8^+$ T cells.

Discussion

Melanoma is one of the most prevalent cancers and has high mortality rates especially after the cancer has metastasized. A high tumor mutational burden (TMB) is strongly correlated with high response and has emerged as a clinically relevant biomarker of CPI efficacy [18,19], however DNA hypomethylation (and demethylation) was strongly correlated with immune evasive and CPI therapy resistant signatures in melanoma, independent of TMB and aneuploidy [21]. In fact, global

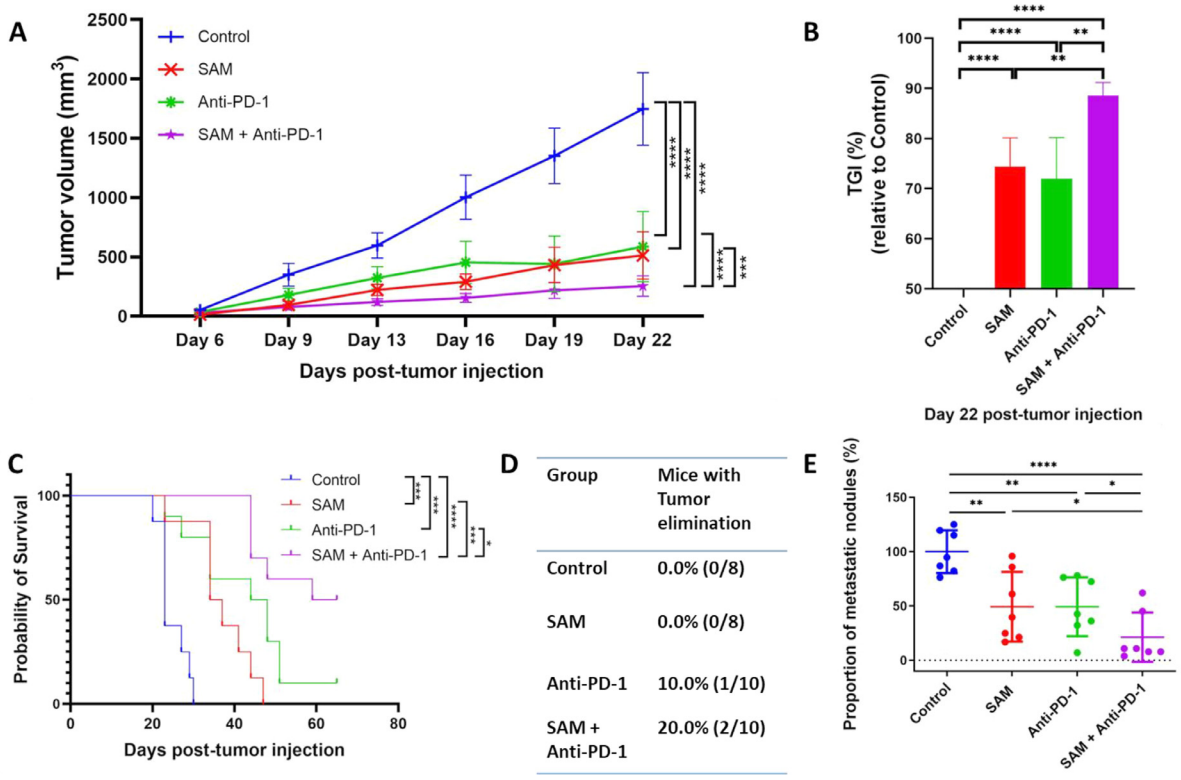

Fig. 6. Combination of SAM with anti-PD-1 antibody results in significant higher anti-cancer efficacy in melanoma mouse models. (A) Tumor volume (mm^3) of control (IgG and PBS), SAM, anti-PD-1 antibody and combination treated YUMMER1.7 (n≥20/group) tumor bearing mice plotted against days post tumor injection. Data pooled from three independent experiments. Essentially, YUMMER1.7 (5×10^5) cells in 20% Matrigel were subcutaneously injected in C57BL/6 mice. When tumors were palpable (day 2-4), treatment was initiated with either control (IgG and PBS), SAM, anti-PD-1 antibody or combination of SAM+anti-PD-1. Tumor volumes (±95% CI) were measured at timed intervals. (B) Percentage tumor growth inhibition (%) (±SEM) of SAM, anti-PD-1 and combination group (n≥20/group) relative to control at Day 22. (C) Kaplan-Meier curve showing the probability of survival of YUMMER1.7 tumor bearing mice in the treated groups (n≥8/group) against days elapsed (or days post-tumor injection). The mice were sacrificed as they reached humane end point (T.V ≥ $2000mm^3$). (D) Table showing the percentage of mice with complete tumor elimination at the end of the study (day 65). (E) Percentage proportion of metastatic nodules (relative to control, ±SEM) on lungs of treated mice at day 15 post-tumor injection. Essentially, B16 (5×10^5) cells were intravenously injected in C57BL/6 mice (n≥ 7/group) and treated with either Control (IgG and PBS), SAM, anti-PD-1 antibody or combination of SAM+anti-PD-1. Statistical significance was calculated using (A) two-way ANOVA test; (C) log-rank test; and (B,E) one-way ANOVA test.

DNA hypomethylation had a higher predictive power than TMB. Furthermore, recent studies have suggested low SAM levels within TME, and deprivation of $CD8^+$ T cells of the precursor of SAM, methionine, makes them non-functional and unresponsive to CPI therapy in melanoma. Thus, we hypothesized that targeting DNA hypomethylation with SAM would be highly beneficial and complement CPI therapy. Here we propose a novel therapeutic strategy by combining SAM with anti-PD-1 antibody to overcome the development of treatment resistance in highly aggressive BRAF mutant and WT melanomas.

During melanogenesis, melanoma cells become less aggressive as genes that repress invasion are upregulated [35,61,62]. In addition, melanosomes were shown to inhibit transmigration ability of melanoma cells mechanistically while melanin pigmentation inhibited metastasis [35,36]. SAM increased the number of cells synthesizing melanin and melanosomes in a dose-dependant manner (Fig. 2). Increase in melanosomes is also indicated by increased expression of *Mitf* which regulates melanosome biogenesis, and genes such as *Tyr* and *Pmel* which are melanosomal structural proteins required for early melanogenesis and melanosome biogenesis (Fig. 3A) [11–14,63]. Indeed, when SAM was tested for metastasis in *in vitro* assays (migration, invasion) and *in vivo* experiments (lung metastasis model), it significantly decreased metastasis of melanoma cells and tumors (Figs. 5D, 6E, Supplementary Fig. 8, and [22]).

MITF regulates expression of many pigmentation, MICs marker, and cell cycle regulatory genes. In a previous study, *MITF* amplification was found to be present in 5-20% of melanomas and *MITF* was defined as a lineage-addiction oncogene [64]. However, targeted-capture deep sequencing has shown no changes in copy number of *MITF* in clinical melanoma samples [65,66]. Furthermore, MITF has demonstrated to suppress melanoma invasion and metastasis, and knock-out/KD of *MITF* increases tumor growth and progression, and metastasis in various melanoma mouse models [9,10,65–69]. MITF acts as a rheostat and dynamically controls phenotype switching and this model is extensively discussed and established [8–10,67,69]. Various studies have indicated that cells expressing low MITF are intrinsically resistant to MAPK pathway inhibitors (such as BRAFi/ MEKi) and immunotherapies (anti-PD-1 and anti-CTLA-4 antibodies), often persist, and have the highest ability to form tumors and metastasize [8,9,67,69–72]. Importantly, dedifferentiated melanomas characterized by low MITF and low MDAs are resistant to immunotherapy as well [15,16,73,74]. Consistently, differentiated dark stained tumors are also infiltrated with higher density of immune cells (immunologically hot) [69]. In addition, tumors with low MITF expression have a pro-inflammatory secretome which ultimately affects recruitment of T cells and function within TME [63]. Interestingly, inhibition of BRAFV600E activity specifically upregulates MITF levels thereby increasing the expression of MDAs which in turn increases immunogenicity of the cancer/tumor cells [75,76]. Indeed, peripheral engineered T cells directed against MDAs led to tumor regression in tumors of human melanoma patients [77]. Recently, a directed phenotype switching was proposed as an effective anti-melanoma strategy

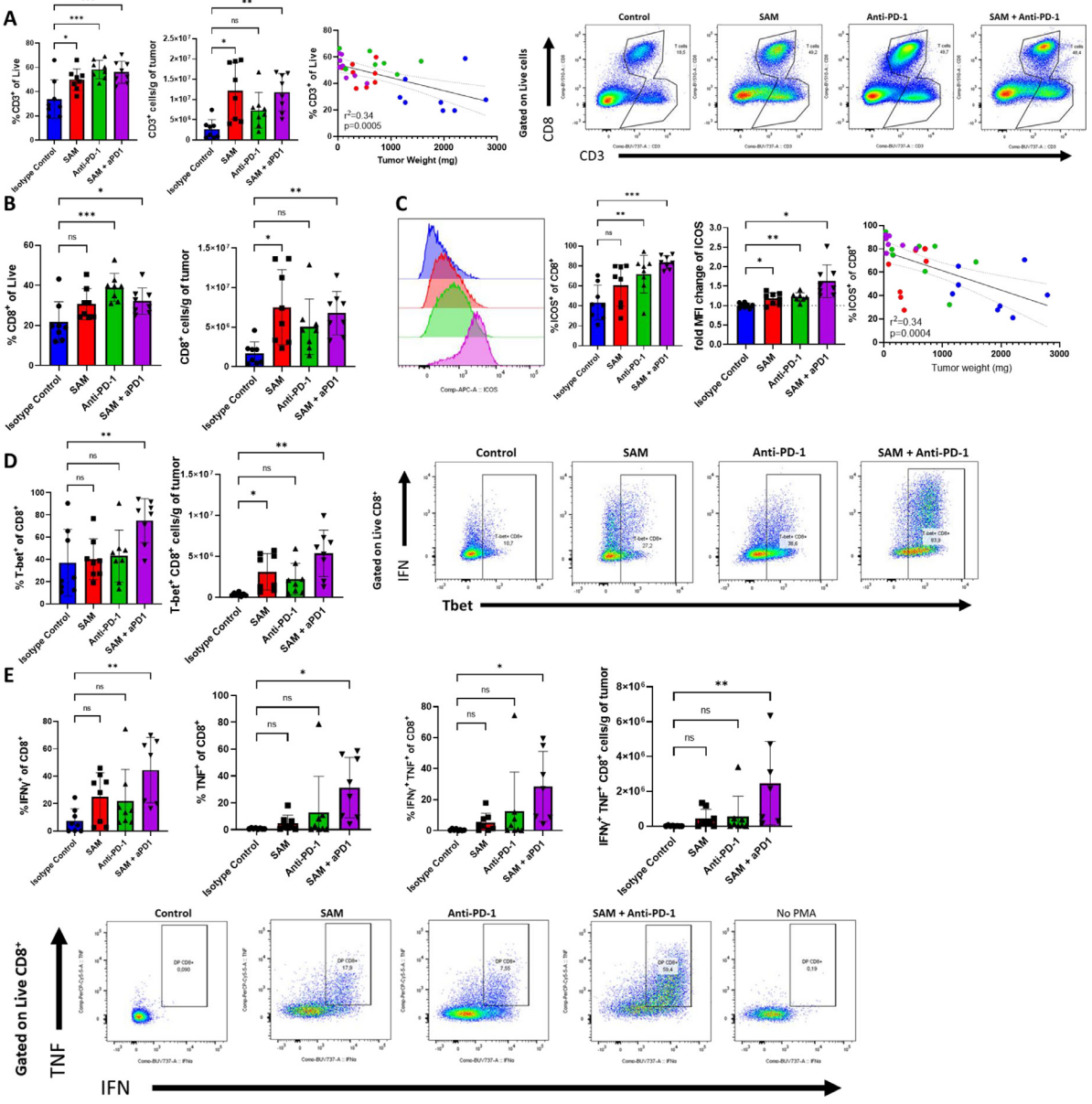

Fig. 7. SAM in combination with anti-PD-1 antibody enhances CD8$^+$ T cells' tumor infiltration, activation, cytokine production and polyfunctionality in the TME. Briefly, YUMMER1.7 tumor-bearing mice were treated with control (isotype matched IgG and PBS), SAM, anti-PD-1 antibody, and combination. At day 22, mice were euthanized, tumors harvested and immunophenotyping by flow cytometry was carried out. (A) Flow cytometry analysis of CD3 and CD8 expression. Representative flow plots gated on live cells. (B) CD8$^+$ T cells frequency (CD8$^+$ CD3$^+$ cell of Live cells) and density (cells per gram of tumor). (C) Flow cytometry analysis of ICOS expression on CD8$^+$ T cells. Representative flow plots of ICOS. Mean fluorescence Intensity (gated on Live CD3$^+$ CD8$^+$ cells). (D) Flow cytometry analysis of T-bet expression. Representative flow plots gated on live CD45$^+$ CD8$^+$ cells. (E) Flow cytometry analysis of IFNγ and TNFα expression (top). Representative flow plots gated on live CD45$^+$ CD8$^+$ cells (bottom). Cells were stimulated for 3h with a cocktail of PMA/Ionomycin/GolgiStop® or cRPMI as control. All histograms are represented as mean ± SD. Statistical significance was calculated using one-way ANOVA test. Data points from all groups were pooled to calculate linear correlations with tumor weight. Treatment groups are indicated by color-coding. The slope's deviation from zero was evaluated using Fisher's test.

by elevating MITF levels and switching the highly proliferative cells and highly invasive cells towards differentiation and cell death [7,9]. Interestingly, SAM causes a similar effect by increasing *Mitf* expression and directing heterogenous proliferative and invasive melanoma cells towards differentiation as indicated by the low proliferation rates, low metastatic ability, melanocyte-like morphology, high melanin and melanosome production, and high MDAs and MAAs expression (Figs. 1–5). Parallel to this, upon examining the TCGA melanoma cohort data, MITF expression strongly mirrored the expression of pigmentation genes that are MITF targets [2]. Hence, low-MITF tumors had low expression of pigmentation genes and vice versa. In line with this, melanosomes contain acidic proteases that degrades proteins into antigenic peptides in the endolysosomal pathways [63]. Since SAM increased number of melanosomes in B16 cells (Fig. 2), this further supports the finding of increased antigen expression of melanoma cells by SAM. Accordingly, SAM treatment had a significant anti-cancer efficacy and reduced tumor growth and progression, and metastasis in immunocompetent models (Figs. 5, 6). Compared to control, SAM treated tumors were also more inflamed (hot) as indicated by an increased T cells infiltration (including CD8$^+$ T cells density, CD4$^+$ T cells density and frequency, and Th17 cells frequency), and higher activation of CD8$^+$ T cells (CD8$^+$ T-bet$^+$/g of tumor and MFI ICOS$^+$) in TME (Figs. 7 and 8).

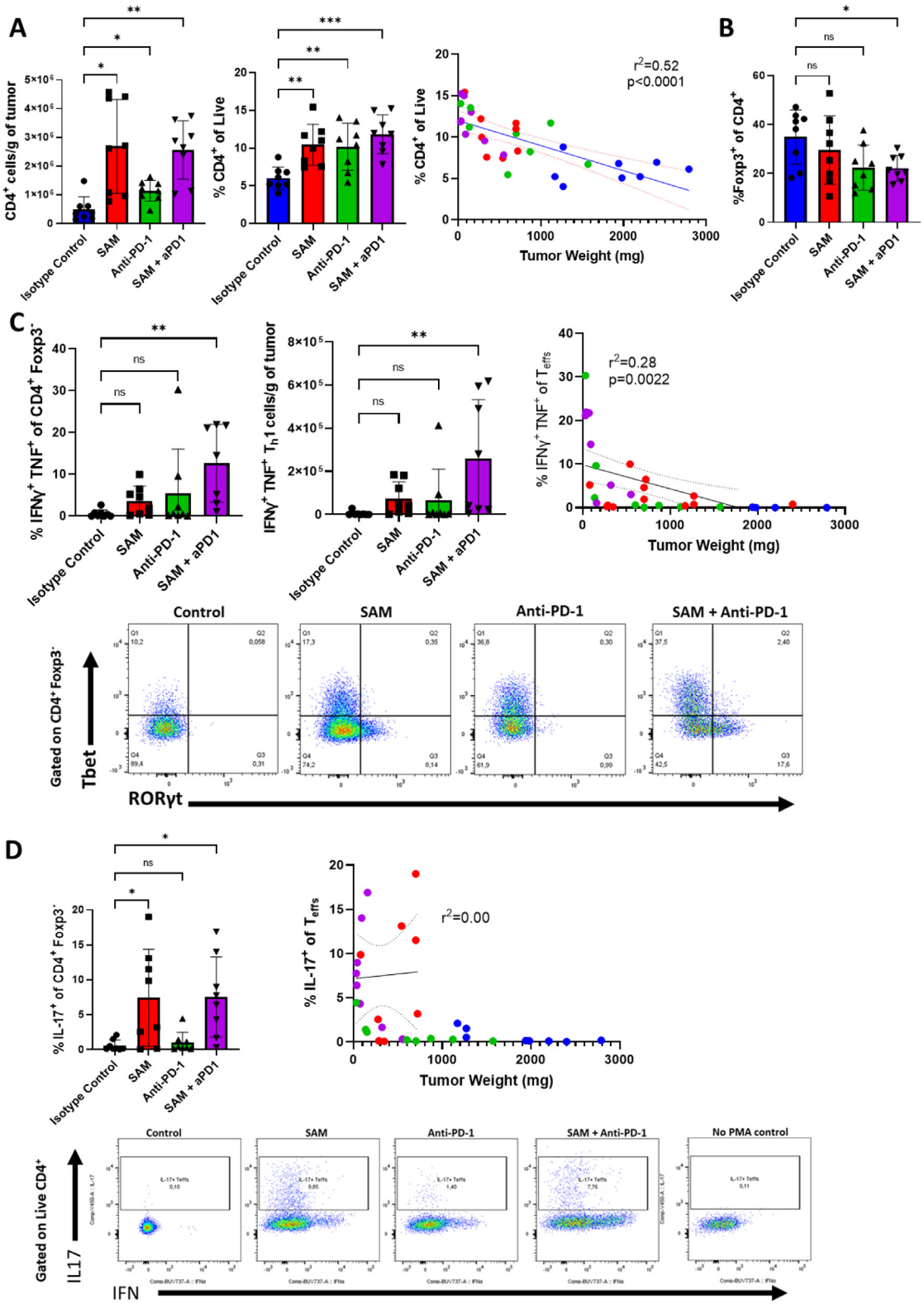

Fig. 8. SAM elevates CD4$^+$ T helper cell responses in the TME. Briefly, YUMMER1.7 tumor-bearing mice were treated with control (isotype matched IgG and PBS), SAM, anti-PD-1 antibody, and combination. At day 22, mice were euthanized, tumors harvested and immunophenotyping by flow cytometry was carried out. (A) Flow cytometry analysis of CD4$^+$ T cells in the TME. Density (cells per g of tumor) of CD4$^+$ T cells; frequency (% CD3$^+$ CD4$^+$ of live cells) of CD4$^+$ T cells; and correlation of CD4$^+$ T cells with tumor weight is presented. (B) Percentage of Foxp3$^+$ of CD4$^+$ T cells. (C) Flow cytometry analysis of T-bet and RORγT expression. Representative flow plots gated on Live CD45$^+$ CD4$^+$ Foxp3$^-$ cells. (D) Flow cytometry analysis of IFNγ and IL-17 expression. Representative flow plots gated on Live CD45$^+$ CD4$^+$ Foxp3$^-$ cells. Cells were stimulated for 3h with a cocktail of PMA/Ionomycin/GolgiStop® or cRPMI as control. All histograms are represented as mean ± SD. Statistical significance was calculated using one-way ANOVA test. Data points from all groups were pooled to calculate linear correlations with tumor weight. Treatment groups are indicated by color-coding. The slope's deviation from zero was evaluated using Fisher's test.

IL6 cytokine production is upregulated by endothelial cells and fibroblasts upon IL17D stimulation [78]. Additionally, IL17D is highly induced by Nrf2 and other stress pathways and can lead to tumor rejection and enhanced anti-cancer immune response [79,80]. Our top significantly upregulated pathways with SAM were Nrf2 and oxidative stress (Supplementary Fig. 2C and 4, and Supplementary Table 6), and SAM increased expression of IL17D (and its receptors) and IL6 (Supplementary Fig. 12). IL17D itself was shown to elevate anti-cancer immune response via NK recruitment [79]. Therefore, Nrf2 pathway inducing IL17D expression and IL6 expression which may then lead to high Th17 cells could be another pathway enhancing immune responses against tumor cells that is induced by SAM. The intriguing effect of SAM on frequency of $IL17^+$ cells in melanoma TME and expression of IL6 and IL17D in melanoma cells will need to be further investigated.

IFNγ is one of the most powerful cytokines that can cause anti-tumor activity, determines the success of CPIs and is a characteristic feature of cytotoxic T cells that produce perforin and granzymes [81–83]. IFNγ has marked anti-tumor pleiotropic effects including inhibition of immunosuppressive T_{regs}, M1 macrophage and $CD4^+$ T_h1 polarization, DCs maturation and MHCI and II upregulation, increased cytotoxic (killing) activity, proliferation, and motility of $CD8^+$ T cells, apoptosis of cancer cells, and inhibition of angiogenesis [81–83]. T-bet regulates the transcription of IFNγ [81]. Similar to IFNγ, TNFα can also cause tumor cell death by apoptosis and inhibit angiogenesis in tumors [83]. Indeed, the greatest reduction in tumor volumes were in the SAM+anti-PD-1 combination group, which is in line with significant upregulation of IFNγ, T-bet and TNFα of cytotoxic $CD8^+$ T cells in these tumors, compared to control. In parallel, there was a trend in increase of IFNγ, T-bet and TNFα by $CD8^+$ T cells with monotherapies which is in line with significant tumor reduction compared to control. Consistently, polyfunctional $CD8^+$ T cells which are the most potent cytotoxic $CD8^+$ T cells and can cause effective tumor lysis, were not present in the control tumors, but were significantly highest in the combination group with a trend in increase in monotherapies (Fig. 7).

A high percentage (>80%) of melanoma patients relapse on the BRAFi/ MEKi cocktail, which is due to, as mentioned above, slow-growing low-MITF-expressing stem-cell like cells [1,2,8,9,67,69–72,84]. Hence, therapies that upregulate MITF can have distinct advantage [7]. Another challenge is that 60–70% of melanoma patients do not respond to CPI therapy [1,5,6,84]. The SAM+anti-PD-1 combination proposed in this study has several advantages: (a) SAM upregulates MITF levels thereby decreasing the pool of slow-growing low-MITF-expressing stem-cell like cells that have high probability of initiating tumors, metastasis, and tumor relapse after treatment. Additionally, SAM increases the immunogenicity, in part by elevating MITF levels, of the melanoma cells. In line with this, we have not found development of pharmacological resistance to long-term treatment of SAM in this study or any other cancer model (*in vitro* and *in vivo*) [22,23,85–87]. (b) While anti-PD-1 antibody has some immune-related adverse effects, SAM being an approved supplement has shown no severe adverse effects in pre-clinical and clinical studies except a transient adverse behavioral effect in an individual [22,23,85–88]. (c) The SAM+anti-PD-1 antibody therapy is effective against both models of BRAF WT and mutant melanoma subtypes which are representative of 80-85% of the melanoma patients. Additionally, we have also observed beneficial effect of the combination in breast cancer [89]. (d) The current study along with our previous published study [22] was conducted using syngeneic melanoma cell lines and immunocompetent mouse tumor models, instead of xenograft models that are severely immune-deficient. Accordingly, these models avoid interspecies immune responses but have a complete immune system against melanoma tumors, therefore, faithfully represent the human pathophysiology that occurs in tumors of human melanoma patients [9,90]. Along these lines, we have used only one CPI (anti-PD-1 antibody) with SAM. This also has advantages compared to the use of drug cocktails such as BRAFi and MEKi with anti-PD-1 and anti-CTLA-4 antibodies currently employed in the clinic which, for example, could have a higher risk of adverse events and more complicated therapeutic regimes. (e) Lastly, SAM+anti-PD-1 antibody combination led to complete tumor elimination in 20% of YUMMER1.7-tumor bearing mice. This is a promising finding which would need further investigation.

Although SAM and anti-PD-1 antibody combination shows significant potential against BRAF mutant and WT melanomas, the current study had some limitations. For instance, since we observed SAM incremented immunogenicity and sensitivity of the melanoma cells *in vitro*, we had started SAM treatment of the tumor-bearing mice at 2-4 days post-tumor inoculation. The rationale behind this was to investigate the effect of SAM on priming the melanoma cells for anti-PD-1 antibody which has been carried out with other epigenetic therapies like DNA methyltransferase inhibitors (DNMTi) and histone deacetylase inhibitors (HDACi) [91,92]. Also, SAM had to be given daily during the treatment period because of low bioavailability of orally taken SAM reported in the past [23,85,88].

Future studies could implement other CPIs with SAM. One promising candidate is anti-CTLA-4 antibody. This is because anti-CTLA-4 antibody elevates the expansion of tumor-infiltrating T_h1 ($PD\text{-}1^+$, $ICOS^+$, $Tbet^+$) cells and $CD8^+$ T cells, and there is some evidence that SAM is required for T cells activation and proliferation [25–29]. Moreover, triple combination of SAM+anti-PD-1+anti-CTLA-4 antibodies could also serve as a potential therapeutic strategy. However, for triple combination therapy, CPI dose would have to be reduced to avoid immune related adverse effects by CPI therapies.

To the best of our knowledge, the current study together with our previous study [22] is the first potential evidence of the beneficial anti-cancer efficacy of SAM against BRAF WT and BRAF mutant melanomas which represent 80-85% of the melanoma patients. Moreover, our studies also to demonstrate the unique anti-cancer therapeutic effects of the novel SAM and anti-PD-1 antibody combination against melanomas. The particularly attractive nature of these studies is that both SAM and anti-PD-1 antibody are approved agents and therefore can be easily translated into the clinic. Of note, a safe and relatively cheap nutritional supplement, SAM, exhibits anti-cancer/anti-metastatic and immune-stimulatory activity which are similar to the effects seen by potentially toxic and more expensive therapies. Our study points out to the potential of this agent in repurposing it for cancer therapy to reduce morbidity and mortality rates of melanoma patients.

Materials and methods

Cell lines

Murine melanoma BRAF mutant YUMM1.7 (RRID:CVCL_JK16) and YUMMER1.7 (RRID:CVCL_A2AX) cell lines were kindly gifted by Dr. Ian Watson (Goodman Cancer Research Centre, McGill University, Montreal, QC, Canada) and Dr. Marcus Bosenberg (Yale University School of Medicine, New Haven, CT, USA), respectively. Human melanoma A375 cell line (RRID:CVCL_0132) was gifted by Dr. Watson as well. Murine B16-F1 (B16) BRAF wild-type (RRID:CVCL_F936) melanoma cell line was obtained from ATCC (Manassas, Virginia). Apart from YUMMER1.7, all cell lines were cultured in DMEM media supplemented with 1% penicillin-streptomycin sulfate and 10% fetal bovine serum (FBS), and 1% non-essential amino acids (NEAA) was also added for YUMM1.7 cells. YUMMER1.7 was cultured in DMEM/F12 media supplemented with 10% FBS, 1%P/S, 1% NEAA. Only early passage cell lines were utilized unless indicated. All cell lines were maintained in incubators at 37°C and 5% CO_2 and found to be mycoplasma-free.

Proliferation and wound-healing assays

For proliferation assays, YUMMER1.7 (1×10^4 cells), YUMM1.7 (0.5×10^4 cells), B16 (1.5×10^4 cells) and A375 (2.5×10^4 cells) were seeded in 6-well plates. The cells were treated with two different concentrations, 200μM and 500μM, of SAM (cat# B9003S, NEB, Canada)

on day 2, 4 and 6 after seeding. On day 7, the cells were collected by trypsinization, neutralized by complete media, and counted with Beckman Coulter counter (Hertfordshire, UK). The cell pellets were either frozen or used for downstream applications. Proliferation assay data is the mean of two independent experiments. Percentage proliferation (%) is calculated as: [(Mean number of cells in (treatment group/ Control group)) x100]. Migration assay followed the regular proliferation assay protocol and then YUMMER1.7 (5×10^4 cells) and A375 (1×10^5 cells) were seeded in a 6-well plate and were confluent on the next day. Next day, the confluent cell layer was scratched in the form of a cross using a 1mL pipette tip. The 6-well plates were kept in IncuCyte® Live-Cell Analysis System and programmed to take images at timed intervals. Confluency tool of the IncuCyte® was used to analyze the closure of width-gap percentage (compared to T= 0 hr) by the migrating cells and plotted using GraphPad Prism.

Analysis of public clinical and molecular data bases

RNA expression data of normal tissue, primary tumors and metastatic tissues of the healthy participants and melanoma patients samples from GTEx and TCGA databases was downloaded using the Xena platform [33] and the data were imported into GraphPad Prism for graph plotting. Xena platform was also used for Kaplan Meier survival plots of human gene expression data (e.g. *FAS* gene).

Melanogenesis experiments

For determining effect of SAM on melanin synthesis, melanin-producing B16 (1.5×10^4) cells were seeded in 6-well plate and followed the regular proliferation assay protocol. On day 7, images were taken at different magnifications using bright-field Olympus microscope (IX51) with DPController software. For intracellular melanin determination, the cells on day 7 were trypsinized, centrifuged, washed with PBS and centrifuged again. Then melanin was extracted from cell pellets by following a slight modification of previously published protocol [93]. Essentially, the cell pellets were treated with 1 N NaOH containing 10% DMSO, vortexed and boiled at 80˚C for 90 minutes, with vortex after every 15 minutes. The cells were then centrifuged, and supernatant was measured at 490nm using Tecan microplate reader. Percentage relative absorbance (relative to control) was calculated and plotted using GraphPad Prism.

RNA extraction, reverse transcription, and quantitative real-time PCR (RT-qPCR)

Total RNA from cells and tumors was extracted using column extraction method utilizing the RNeasy mini kit (cat# 71404, Qiagen, Germany) and following company's guidelines. The RNA was quantified using BioDrop analyzer according to manufacturer's instructions. For reverse transcription of RNA into cDNA standard thermal cycler was utilized with M-MLV Reverse Transcriptase (cat# 28025013, ThermoFisher Scientific, Canada) enzyme following standard company's guidelines. Then, quantitative real-time qPCR system (AB StepOnePlus) with PowerUp™ SYBR™ Green Master Mix (cat# A25742, ThermoFisher Scientific, Canada) was used to obtain Ct values according to the manufacturer's instructions [22,85]. Analysis of gene expression was carried out using the 2-ΔΔCT method. Primers are tabulated in Supplementary Table 1.

RNA sequencing and bioinformatics analysis

Total RNA was extracted from cells and checked for quality control (QC) by Bioanalyzer (Agilent) and NanoDrop where only RNA Integrity Number (RIN) >6.5 and an absorbance A260/280 ratio of >2.0 was used for RNA-seq. Paired-end RNA sequencing using Illumina NovaSeq 6000 platform (with a depth of 25 million reads) following standard protocols was carried out. The obtained data was checked for QC, normalized, converted into HT-seq count files, and differential gene expression analysis carried out using DESeq2 (RRID:SCR_015687) in Galaxy (www.usegalaxy.org) according to writer's recommendations [94]. The final gene list was annotated using the Annotation tool ("Annotate DESeq2/DEXSeq output tables"). Pathway analysis was carried out using SeqGSEA software (RRID:SCR_005724) [95,96].

siRNA knock-down (KD) experiments

siRNAs for Mitf (cat# sc-35935, Santa Cruz Biotechnology, US) containing 3 different siMitf targeting different exons of Mitf were utilized to KD the Mitf mRNA expression. KD of Mitf mouse gene was carried out using Lipofectamine™ 2000 Transfection Reagent and Opti-MEM™ (ThermoFisher Scientific, Canada) using manufacturer's standard protocol. SiScr (siRNA-A, cat# sc-37007, Santa Cruz Biotechnology, US) was used as a negative control. For Mitf KD confirmation, cells were trypsinized and total RNA was isolated after 48hrs of transfection.

Mouse studies

Male C57BL/6 mice (RRID:IMSR_CRL:027), six to eight weeks of age, were purchased from Charles River Lab (QC, Canada) and housed at ARD division of the RI-MUHC (Montreal, QC, Canada). To generate tumors, 5×10^5 YUMMER1.7 (in 20% Matrigel and 80% saline), and 5×10^5 B16 cells (in saline), were subcutaneously injected into the shaved right flank of mice. Mice were randomized into four groups; control (IgG and PBS); SAM; anti-PD-1 antibody; and SAM+anti-PD-1 antibody combination. When tumor became palpable (2-4 days), treatments were started wherein SAM (Life Science Laboratories, NJ, US) at 80mg/kg dose was diluted in PBS and given daily via oral gavage using feeding needles [22,85]. Anti-PD-1 antibody (clone RMP1-14, BioXCell cat# BE0146, RRID:AB_10949053) and isotype matched control IgG (IgG2a, clone 2A3, BioXcell, cat# BE0089, RRID:AB_1107769) was given at 10mg/kg via intra-peritoneal (i.p.) injection twice a week and diluted in *InVivo*Pure pH 7.0 Dilution Buffer (BioXcell, US) [22,85]. The control mice were also given PBS via oral gavage. Measurement of tumor volume (T.V) was carried out by palpation using a digital calliper at timed intervals and determined using the formula; $T.V = (\text{length} \times \text{width}^2)/2$. Tumor growth inhibition percentage (%) was calculated as ((1 – [changes of T.V in treatment group/changes of T.V in control group] × 100) [97]. For survival studies, the YUMMER1.7 tumor bearing mice (n≥ 8/group) were treated with anti-PD-1 antibody until day 22 and continued SAM treatment until the end of the study (day 65). The mice were euthanized as their tumors reached humane endpoint (a T.V of ≥2000mm^3). The data for survival studies was plotted with Kaplan Meier curve using GraphPad Prism. For generating pulmonary metastasis mouse model of melanoma, B16 (5×10^5) cells were intravenously injected (I.V) into the tail vein of the C57BL/6 mice (n= 7/group) and treated with either control (IgG and PBS), SAM, anti-PD-1 antibody, or SAM+anti-PD-1 antibody combination. The mice were euthanized at day 15 post tumor injection, lungs harvested and fixed with formalin solution, and metastatic lung nodules counted. Percentage proportion of metastatic nodules (%) was calculated relative to control as ([total lung nodules in treatment group/ mean lung nodules in control group] × 100). Mice were regularly examined physically, measuring body weight, and for other potential adverse effects [98]. All mouse studies were carried out under standard conditions and in accordance with McGill University Facility Animal Care Committee guidelines.

Immunophenotyping

Immunophenotyping was carried out to study the effect that SAM and anti-PD-1 antibody has on immune cells within TME. Briefly,

YUMMER1.7-tumor bearing mice (n=8/group) were treated with either control (isotype matched IgG and PBS), SAM, anti-PD-1 antibody, or combination. The mice were sacrificed, primary tumors were harvested, processed into single cell suspensions, and stained with extracellular and intracellular markers and cytokines as previously detailed by us [22]. Samples were then acquired using the BD Fortessa LSR-X20 and analysis was performed using FlowJo (RRID:SCR_008520) [22,99]. All fluorescence-conjugated antibodies utilized for flow cytometry are tabulated in Supplementary Table 2.

Immunohistochemistry (IHC)

Tumors treated with control and SAM were harvested at endpoint (n=4/group). Tumors were fixed with formalin for 3-5 days and washed with 70% ethanol. An automated IHC was performed on Ventana Discovery Ultra Instrument (Roche, US). Slides were deparaffinized and rehydrated, treated with EDTA buffer for antigen retrieval and then incubated with mouse anti-Ki67 antibody (Abcam cat# ab15580, RRID:AB_443209) at 1:300 dilution. Then, anti-rabbit horseradish peroxidase (HRP)-conjugated secondary antibody was added, and signal detected using DAB chromogen kit (Biocare Medical). Slides were counter stained with Haemotoxylin and Eosin (H&E). Slides were scanned with Aperio AT Turbo digital. Images (at 40x magnification) of the ki67 stained slides were taken (n=5 images/sample) randomly using ImageScope (RRID:SCR_014311) and analyzed using Fiji (RRID:SCR_002285). In Fiji, a colour deconvolution tool was utilized to separate H&E (total cell stain) and DAB (ki67$^+$ stain) sections, and then using analyze particles tool, optimal total area of H&E and DAB staining was carried out. Then a macro was created that automatically carried out the above for one image. Then the images were input one by one for each sample into the macro. Percentage of ki67 staining was calculated as [total area of ((DAB/H&E) staining) x100%)] and was plotted using GraphPad Prism (RRID:SCR_002798).

Statistical analysis

Significance testing was determined by two-tailed Student's t-test or one-way/two-way ANOVA using GraphPad Prism (RRID:SCR_002798). Significance values are represented by asterisks ($^*p < 0.05$; $^{**}p < 0.01$, $^{***}p < 0.001$ and $^{****}p < 0.0001$).

Data availability statement

The data analyzed or generated is available within the main file and in the supplementary files.

Ethics statement

Guidelines of the Facility Animal Care Committee (FACC) of McGill University were followed for all animal studies.

Declaration of Competing Interest

The authors declare that they have no known competing financial interests or personal relationships that could have appeared to influence the work reported in this paper.

CRediT authorship contribution statement

A. Mehdi: Conceptualization, Data curation, Formal analysis, Investigation, Methodology, Software, Validation, Visualization, Writing – original draft, Writing – review & editing. **M. Attias:** Data curation, Formal analysis, Investigation, Visualization, Writing – review & editing. **A. Arakelian:** Investigation, Validation. **M. Szyf:** Supervision, Writing – review & editing. **C.A. Piccirillo:** Data curation, Funding acquisition, Supervision, Writing – review & editing. **S.A. Rabbani:** Conceptualization, Funding acquisition, Resources, Supervision, Writing – review & editing.

Acknowledgements and Funding

The study was supported by the Canadian Institutes of Health Research (CIHR) grants, PJT-156225 and PJT-148821, awarded to Shafaat A. Rabbani and Ciriaco A. Piccirillo, respectively. Ali Mehdi is recipient of Fonds de recherche du Québec – Santé (FRQ-S) scholarship.

Supplementary materials

Supplementary material associated with this article can be found, in the online version, at doi:10.1016/j.neo.2022.100874.

References

[1] D. Schadendorf, et al., Melanoma, Lancet 392 (10151) (2018) 971–984.
[2] T.C.G.A. Network, Genomic Classification of Cutaneous Melanoma, Cell 161 (7) (2015) 1681–1696.
[3] A. Rogiers, et al., Long-Term Survival, Quality of Life, and Psychosocial Outcomes in Advanced Melanoma Patients Treated with Immune Checkpoint Inhibitors, J Oncol 2019 (2019) 5269062.
[4] R. Asmar, J. Yang, R.D. Carvajal, Clinical utility of nivolumab in the treatment of advanced melanoma, Ther Clin Risk Manag 12 (2016) 313–325.
[5] A. Kalbasi, A. Ribas, Tumour-intrinsic resistance to immune checkpoint blockade, Nat Rev Immunol 20 (1) (2020) 25–39.
[6] L. Barrueto, et al., Resistance to Checkpoint Inhibition in Cancer Immunotherapy, Transl Oncol 13 (3) (2020) 100738.
[7] M. Saez-Ayala, et al., Directed phenotype switching as an effective antimelanoma strategy, Cancer Cell 24 (1) (2013) 105–119.
[8] F. Rambow, J.C. Marine, C.R. Goding, Melanoma plasticity and phenotypic diversity: therapeutic barriers and opportunities, Genes Dev, 33 (19-20) (2019) 1295–1318.
[9] Y. Cheli, et al., Mitf is the key molecular switch between mouse or human melanoma initiating cells and their differentiated progeny, Oncogene 30 (20) (2011) 2307–2318.
[10] K.S. Hoek, et al., In vivo switching of human melanoma cells between proliferative and invasive states, Cancer Res 68 (3) (2008) 650–656.
[11] S.A. D'Mello, et al., Signaling Pathways in Melanogenesis, Int J Mol Sci 17 (7) (2016).
[12] S. Page, V. Chandhoke, A. Baranova, Melanin and melanogenesis in adipose tissue: possible mechanisms for abating oxidative stress and inflammation? Obes Rev 12 (5) (2011) e21–e31.
[13] C. Levy, M. Khaled, D.E. Fisher, MITF: master regulator of melanocyte development and melanoma oncogene, Trends Mol Med 12 (9) (2006) 406–414.
[14] J. Pitcovski, et al., Melanoma antigens and related immunological markers, Crit Rev Oncol Hematol 115 (2017) 36–49.
[15] J. Landsberg, et al., Melanomas resist T-cell therapy through inflammation-induced reversible dedifferentiation, Nature 490 (7420) (2012) 412–416.
[16] F. Huang, et al., Inhibiting the MNK1/2-eIF4E axis impairs melanoma phenotype switching and potentiates antitumor immune responses, J Clin Invest (8) (2021) 131.
[17] G.L. Beatty, W.L. Gladney, Immune escape mechanisms as a guide for cancer immunotherapy, Clin Cancer Res 21 (4) (2015) 687–692.
[18] L.B. Alexandrov, et al., Signatures of mutational processes in human cancer, Nature 500 (7463) (2013) 415–421.
[19] M. Yarchoan, A. Hopkins, E.M. Jaffee, Tumor Mutational Burden and Response Rate to PD-1 Inhibition, N Engl J Med 377 (25) (2017) 2500–2501.
[20] S. Romero-Garcia, H. Prado-Garcia, A. Carlos-Reyes, Role of DNA Methylation in the Resistance to Therapy in Solid Tumors, Front Oncol 10 (2020) 1152.
[21] H. Jung, et al., DNA methylation loss promotes immune evasion of tumours with high mutation and copy number load, Nat Commun 10 (1) (2019) 4278.
[22] A. Mehdi, et al., Enhanced Anticancer Effect of a Combination of S-adenosylmethionine (SAM) and Immune Checkpoint Inhibitor (ICPi) in a Syngeneic Mouse Model of Advanced Melanoma, Front Oncol 10 (2020) 1361.
[23] N. Mahmood, et al., An enhanced chemopreventive effect of methyl donor S-adenosylmethionine in combination with 25-hydroxyvitamin D in blocking mammary tumor growth and metastasis, Bone Res 8 (2020) 28.
[24] T. Bottiglieri, S-Adenosyl-L-methionine (SAMe): from the bench to the bedside—molecular basis of a pleiotrophic molecule, Am J Clin Nutr 76 (5) (2002) 1151S–11517S.
[25] P.T. Hote, et al., Ethanol inhibits methionine adenosyltransferase II activity and S-adenosylmethionine biosynthesis and enhances caspase-3-dependent cell death in T lymphocytes: relevance to alcohol-induced immunosuppression, J Nutr Biochem 19 (6) (2008) 384–391.
[26] R. Tobena, et al., Interleukin-2 induces gamma-S-adenosyl-L-methionine synthetase gene expression during T-lymphocyte activation, Biochem J 319 (Pt 3) (1996) 929–933.
[27] Jr H.L. LeGros, A.M. Geller, M. Kotb, Differential regulation of methionine adenosyltransferase in superantigen and mitogen stimulated human T lymphocytes, J Biol Chem 272 (25) (1997) 16040–16047.

[28] M. Kotb, J.B. Dale, E.H. Beachey, Stimulation of S-adenosylmethionine synthetase in human lymphocytes by streptococcal M protein, J Immunol 139 (1) (1987) 202–206.
[29] J. De La Rosa, et al., Induction of interleukin 2 production but not methionine adenosyltransferase activity or S-adenosylmethionine turnover in Jurkat T-cells, Cancer Res 52 (12) (1992) 3361–3366.
[30] Y. Bian, et al., Cancer SLC43A2 alters T cell methionine metabolism and histone methylation, Nature (2020).
[31] O.A. Ulanovskaya, A.M. Zuhl, B.F. Cravatt, NNMT promotes epigenetic remodeling in cancer by creating a metabolic methylation sink, Nat Chem Biol 9 (5) (2013) 300–306.
[32] D. Hanahan, R.A. Weinberg, Hallmarks of cancer: the next generation, Cell 144 (5) (2011) 646–674.
[33] M.J. Goldman, et al., Visualizing and interpreting cancer genomics data via the Xena platform, Nat Biotechnol 38 (6) (2020) 675–678.
[34] D. Zhang, et al., MGDB: a comprehensive database of genes involved in melanoma, Database (Oxford) 2015 (2015).
[35] M. Sarna, et al., Melanin presence inhibits melanoma cell spread in mice in a unique mechanical fashion, Sci Rep 9 (1) (2019) 9280.
[36] M. Sarna, et al., Cell elasticity is an important indicator of the metastatic phenotype of melanoma cells, Exp Dermatol 23 (11) (2014) 813–818.
[37] W.W. Overwijk, N.P. Restifo, B16 as a mouse model for human melanoma, Curr Protoc Immunol, (2001) **Chapter 20**Unit 20.1.
[38] T. Hirobe, et al., Effects of fibroblast-derived factors on the proliferation and differentiation of human melanocytes in culture, J Dermatol Sci 71 (1) (2013) 45–57.
[39] M. Cichorek, et al., Skin melanocytes: biology and development, Postepy Dermatol Alergol 30 (1) (2013) 30–41.
[40] K.S. Hoek, et al., Novel MITF targets identified using a two-step DNA microarray strategy, Pigment Cell Melanoma Res 21 (6) (2008) 665–676.
[41] M. Perego, et al., Heterogeneous phenotype of human melanoma cells with in vitro and in vivo features of tumor-initiating cells, J Invest Dermatol 130 (7) (2010) 1877–1886.
[42] G. Parmiani, Melanoma Cancer Stem Cells: Markers and Functions, Cancers (Basel) 8 (3) (2016).
[43] C. Friesen, et al., Involvement of the CD95 (APO-1/FAS) receptor/ligand system in drug-induced apoptosis in leukemia cells, Nat Med 2 (5) (1996) 574–577.
[44] M. Hahne, et al., Melanoma cell expression of Fas(Apo-1/CD95) ligand: implications for tumor immune escape, Science 274 (5291) (1996) 1363–1366.
[45] C. Dostert, et al., The TNF Family of Ligands and Receptors: Communication Modules in the Immune System and Beyond, Physiol Rev 99 (1) (2019) 115–160.
[46] H. Helmbach, et al., Drug-resistance in human melanoma, Int J Cancer 93 (5) (2001) 617–622.
[47] L. Cai, et al., Role of inhibitor of growth 4 in the suppression of human melanoma cells through the Fas/FasL-mediated apoptosis pathway, Int J Mol Med 41 (2) (2018) 1055–1061.
[48] R. Upadhyay, et al., A Critical Role for Fas-Mediated Off-Target Tumor Killing in T-cell Immunotherapy, Cancer Discov 11 (3) (2021) 599–613.
[49] D. Cho, et al., Endogenous interleukin-18 modulates immune escape of murine melanoma cells by regulating the expression of Fas ligand and reactive oxygen intermediates, Cancer Res 60 (10) (2000) 2703–2709.
[50] M.J. Deeths, M.F. Mescher, ICAM-1 and B7-1 provide similar but distinct costimulation for CD8+ T cells, while CD4+ T cells are poorly costimulated by ICAM-1, Eur J Immunol 29 (1) (1999) 45–53.
[51] P. Shier, K. Ngo, W.P. Fung-Leung, Defective CD8+ T cell activation and cytolytic function in the absence of LFA-1 cannot be restored by increased TCR signaling, J Immunol 163 (9) (1999) 4826–4832.
[52] C. Blank, et al., ICAM-1 contributes to but is not essential for tumor antigen cross-priming and CD8+ T cell-mediated tumor rejection in vivo, J Immunol 174 (6) (2005) 3416–3420.
[53] A.T. Lefor, D.F. Fabian, Enhanced cytolytic activity of tumor infiltrating lymphocytes (TILs) derived from an ICAM-1 transfected tumor in a murine model, J Surg Res 75 (1) (1998) 49–53.
[54] W.M. Sartor, et al., Enhanced expression of ICAM-1 in a murine fibrosarcoma reduces tumor growth rate, J Surg Res 59 (1) (1995) 66–74.
[55] L.T. Li, et al., Ki67 is a promising molecular target in the diagnosis of cancer (review), Mol Med Rep 11 (3) (2015) 1566–1572.
[56] D.M. Pardoll, The blockade of immune checkpoints in cancer immunotherapy, Nature Reviews Cancer 12 (4) (2012) 252.
[57] F. Wimmers, et al., Long-lasting multifunctional CD8(+) T cell responses in end-stage melanoma patients can be induced by dendritic cell vaccination, Oncoimmunology 5 (1) (2016) e1067745.
[58] A. Saran, et al., Loss of tyrosinase activity confers increased skin tumor susceptibility in mice, Oncogene 23 (23) (2004) 4130–4135.
[59] G.J. Prud'homme, Pathobiology of transforming growth factor beta in cancer, fibrosis and immunologic disease, and therapeutic considerations, Lab Invest 87 (11) (2007) 1077–1091.
[60] N. Martin-Orozco, et al., T helper 17 cells promote cytotoxic T cell activation in tumor immunity, Immunity 31 (5) (2009) 787–798.
[61] K.S. Hoek, et al., Metastatic potential of melanomas defined by specific gene expression profiles with no BRAF signature, Pigment Cell Res 19 (4) (2006) 290–302.
[62] S. Carreira, et al., Mitf regulation of Dia1 controls melanoma proliferation and invasiveness, Genes Dev 20 (24) (2006) 3426–3439.
[63] R. Ballotti, Y. Cheli, C. Bertolotto, The complex relationship between MITF and the immune system: a Melanoma ImmunoTherapy (response) Factor? Mol Cancer 19 (1) (2020) 170.
[64] L.A. Garraway, et al., Integrative genomic analyses identify MITF as a lineage survival oncogene amplified in malignant melanoma, Nature 436 (7047) (2005) 117–122.
[65] M.L. Hartman, M. Czyz, Pro-survival role of MITF in melanoma, J Invest Dermatol 135 (2) (2015) 352–358.
[66] K. Harbst, et al., Molecular and genetic diversity in the metastatic process of melanoma, J Pathol 233 (1) (2014) 39–50.
[67] Y. Cheli, et al., Hypoxia and MITF control metastatic behaviour in mouse and human melanoma cells, Oncogene 31 (19) (2012) 2461–2470.
[68] R.E. Bell, et al., Transcription factor/microRNA axis blocks melanoma invasion program by miR-211 targeting NUAK1, J Invest Dermatol 134 (2) (2014) 441–451.
[69] G.M. Wiedemann, et al., Microphthalmia-Associated Transcription Factor (MITF) Regulates Immune Cell Migration into Melanoma, Transl Oncol 12 (2) (2019) 350–360.
[70] R. Dilshat, et al., MITF reprograms the extracellular matrix and focal adhesion in melanoma, Elife 10 (2021).
[71] F. Rambow, et al., Toward Minimal Residual Disease-Directed Therapy in Melanoma, Cell 174 (4) (2018) 843–855 e19.
[72] J. Travnickova, et al., Zebrafish MITF-Low Melanoma Subtype Models Reveal Transcriptional Subclusters and MITF-Independent Residual Disease, Cancer Res 79 (22) (2019) 5769–5784.
[73] A. Mehta, et al., Immunotherapy Resistance by Inflammation-Induced Dedifferentiation, Cancer Discov 8 (8) (2018) 935–943.
[74] N. Srour, et al., PRMT7 ablation stimulates anti-tumor immunity and sensitizes melanoma to immune checkpoint blockade, Cell Rep 38 (13) (2022) 110582.
[75] J.J. Hsiao, D.E. Fisher, The roles of microphthalmia-associated transcription factor and pigmentation in melanoma, Arch Biochem Biophys 563 (2014) 28–34.
[76] A. Boni, et al., Selective BRAFV600E inhibition enhances T-cell recognition of melanoma without affecting lymphocyte function, Cancer Res 70 (13) (2010) 5213–5219.
[77] L.A. Johnson, et al., Gene therapy with human and mouse T-cell receptors mediates cancer regression and targets normal tissues expressing cognate antigen, Blood 114 (3) (2009) 535–546.
[78] T. Starnes, et al., Cutting edge: IL-17D, a novel member of the IL-17 family, stimulates cytokine production and inhibits hemopoiesis, J Immunol 169 (2) (2002) 642–646.
[79] T. O'Sullivan, et al., Interleukin-17D mediates tumor rejection through recruitment of natural killer cells, Cell Rep 7 (4) (2014) 989–998.
[80] R. Saddawi-Konefka, et al., Nrf2 Induces IL-17D to Mediate Tumor and Virus Surveillance, Cell Rep 16 (9) (2016) 2348–2358.
[81] D. Jorgovanovic, et al., Roles of IFN-gamma in tumor progression and regression: a review, Biomark Res 8 (2020) 49.
[82] P. Bhat, et al., Interferon-gamma derived from cytotoxic lymphocytes directly enhances their motility and cytotoxicity, Cell Death Dis 8 (6) (2017) e2836.
[83] J. Shen, et al., Anti-cancer therapy with TNFalpha and IFNgamma: A comprehensive review, Cell Prolif 51 (4) (2018) e12441.
[84] V.W. Rebecca, R. Somasundaram, M. Herlyn, Pre-clinical modeling of cutaneous melanoma, Nat Commun 11 (1) (2020) 2858.
[85] N. Mahmood, et al., Methyl donor S-adenosylmethionine (SAM) supplementation attenuates breast cancer growth, invasion, and metastasis in vivo; therapeutic and chemopreventive applications, Oncotarget 9 (4) (2018) 5169–5183.
[86] N. Mahmood, S.A. Rabbani, Targeting DNA Hypomethylation in Malignancy by Epigenetic Therapies, Adv Exp Med Biol 1164 (2019) 179–196.
[87] S. Parashar, et al., S-adenosylmethionine blocks osteosarcoma cells proliferation and invasion in vitro and tumor metastasis in vivo: therapeutic and diagnostic clinical applications, Cancer Med 4 (5) (2015) 732–744.
[88] J.L. Goren, et al., Bioavailability and lack of toxicity of S-adenosyl-L-methionine (SAMe) in humans, Pharmacotherapy 24 (11) (2004) 1501–1507.
[89] A. Mehdi, et al., Co-Targeting Luminal B Breast Cancer with S-Adenosylmethionine and Immune Checkpoint Inhibitor Reduces Primary Tumor Growth and Progression, and Metastasis to Lungs and Bone, Cancers 15 (1) (2023) 48.
[90] C. Bertolotto, et al., Microphthalmia gene product as a signal transducer in cAMP-induced differentiation of melanocytes, J Cell Biol 142 (3) (1998) 827–835.
[91] A. Mehdi, S.A. Rabbani, Role of Methylation in Pro- and Anti-Cancer Immunity, Cancers (Basel) 13 (3) (2021).
[92] J. Dunn, S. Rao, Epigenetics and immunotherapy: The current state of play, Mol Immunol 87 (2017) 227–239.
[93] S. Chung, G.J. Lim, J.Y. Lee, Quantitative analysis of melanin content in a three-dimensional melanoma cell culture, Sci Rep 9 (1) (2019) 780.
[94] M.I. Love, W. Huber, S. Anders, Moderated estimation of fold change and dispersion for RNA-seq data with DESeq2, Genome Biol 15 (12) (2014) 550.
[95] V.K. Mootha, et al., PGC-1alpha-responsive genes involved in oxidative phosphorylation are coordinately downregulated in human diabetes, Nat Genet 34 (3) (2003) 267–273.
[96] A. Subramanian, et al., Gene set enrichment analysis: a knowledge-based approach for interpreting genome-wide expression profiles, Proc Natl Acad Sci U S A, 102 (43) (2005) 15545–15550.
[97] P. Ubezio, Beyond The T/C Ratio: Old And New Anticancer Activity Scores In Vivo, Cancer Manag Res 11 (2019) 8529–8538.
[98] L. Rastelli, et al., A KDR-binding peptide (ST100,059) can block angiogenesis, melanoma tumor growth and metastasis in vitro and in vivo, Int J Oncol 39 (2) (2011) 401–408.
[99] A. Cossarizza, et al., Guidelines for the use of flow cytometry and cell sorting in immunological studies (second edition), Eur J Immunol 49 (10) (2019) 1457–1973.